



ALMA MATER STUDIORUM  
UNIVERSITÀ DI BOLOGNA

ARCHIVIO ISTITUZIONALE  
DELLA RICERCA

## Alma Mater Studiorum Università di Bologna Archivio istituzionale della ricerca

Seismic-induced damage in historical masonry vaults: A case-study in the 2012 Emilia earthquake-stricken area

This is the final peer-reviewed author's accepted manuscript (postprint) of the following publication:

*Published Version:*

Seismic-induced damage in historical masonry vaults: A case-study in the 2012 Emilia earthquake-stricken area / Antonio Maria D'Altri, Giovanni Castellazzi, Stefano de Miranda, Antonio Tralli. - In: JOURNAL OF BUILDING ENGINEERING. - ISSN 2352-7102. - ELETTRONICO. - 13:(2017), pp. 224-243. [10.1016/j.job.2017.08.005]

*Availability:*

This version is available at: <https://hdl.handle.net/11585/621910> since: 2020-04-08

*Published:*

DOI: <http://doi.org/10.1016/j.job.2017.08.005>

*Terms of use:*

Some rights reserved. The terms and conditions for the reuse of this version of the manuscript are specified in the publishing policy. For all terms of use and more information see the publisher's website.

This item was downloaded from IRIS Università di Bologna (<https://cris.unibo.it/>).  
When citing, please refer to the published version.

(Article begins on next page)

This is the final peer-reviewed accepted manuscript of:

Antonio Maria D'Altri, Giovanni Castellazzi, Stefano de Miranda, Antonio Tralli,  
*Seismic-induced damage in historical masonry vaults: A case-study in the 2012 Emilia  
earthquake-stricken area*, Journal of Building Engineering, Volume 13, 2017, Pages  
224-243

ISSN 2352-7102

The final published version is available online at:

<https://doi.org/10.1016/j.jobe.2017.08.005>

© 2017. This manuscript version is made available under the Creative Commons Attribution-NonCommercial-NoDerivs (CC BY-NC-ND) 4.0 International License  
(<http://creativecommons.org/licenses/by-nc-nd/4.0/>)

# Seismic-induced damage in historical masonry vaults: a case-study in the 2012 Emilia earthquake-stricken area

Antonio Maria D'Altri<sup>1\*</sup>, Giovanni Castellazzi<sup>1</sup>, Stefano de Miranda<sup>1</sup>, Antonio Tralli<sup>2</sup>

<sup>1</sup> *Department of Civil, Chemical, Environmental, and Materials Engineering (DICAM), University of Bologna, Viale del Risorgimento 2, 40136 Bologna, Italy*

<sup>2</sup> *Engineering Department, University of Ferrara, Via Saragat 1, 44122 Ferrara, Italy*

---

## Abstract

The seismic analysis of historical masonry vaults is a challenging task for contemporary engineers as their behavior depends on a very huge number of factors. Among them, the vaults response is also influenced by the seismic behavior of their bearing structures. This paper aims at investigating the capabilities and **limitations** of current finite element-based computational tools to analyze the seismic-induced damage in masonry vaulted structures. The case under study is the Giulio II vault, located in the main tower of the San Felice sul Panaro fortress (Italy) which has been severely damaged by the 2012 Emilia earthquake. Much attention is focused on the interaction between the vault and its bearing tower. The developed finite element model includes the 3D geometry of the vault within the geometry of the tower, based on a before-quake survey. Nonlinear static and dynamic analyses are carried out by using a damage-plasticity constitutive law for masonry. Numerical results are compared to the vault actual crack pattern as well as to its actual-deformed geometry based on a post-quake laser scanner survey.

*Keywords:* Historical masonry vaults, Seismic damage, FE nonlinear analysis, Architectural Heritage, Laser scanner

---

## 1. Introduction

The disasters caused by past and recent earthquakes on both monumental and ordinary historical masonry buildings have induced many researchers to investigate their seismic behavior. Most of the research works were focused on studying the seismic response of vertical masonry structures [1, 2], or to analyze entire buildings also taking into account horizontal structural elements, generally constituted by timber floors or masonry vaults. In particular, these latter elements have been studied aiming at investigating their role in the seismic response of buildings. Indeed, working as horizontal diaphragms, their behavior significantly affects the overall response of the structure in terms of both strength and stiffness [3]. **However**, as their collapse may cause casualties and large artistic and cultural losses (e.g. the

---

\*corresponding author: antoniomaria.daltri2@unibo.it

33 collapse of two frescoed vaults of the upper Basilica of St Francis of Assisi in 1997 [5]), deep  
34 investigations of their response under earthquake actions appear of primary importance.  
35 The seismic analysis of historical masonry vaults is a challenging task for contemporary  
36 engineers as their behavior depends on a very huge number of factors. Among them, the  
37 vaults response is also influenced by the seismic behavior of their bearing structures.

38 Another aspect which further makes challenging this topic derives from the complex ge-  
39 ometries that characterize masonry vaulted structures. Recently, advanced surveying tech-  
40 niques, such as laser scanner, allow to rapidly capture the detailed geometry of complex  
41 objects. This technology has been successfully used for generating 3D models and monitor-  
42 ing the deformations of very complex masonry domes, see for instance [4].

43 Several studies have been dedicated to the analysis of masonry vaults under static verti-  
44 cal actions. Following [6] or [7], it can be affirmed that the modern theory of limit analysis  
45 of masonry structures, which has been developed mainly by Heyman [8, 9], is the most  
46 reliable tool to understand and analyze masonry curved structures. However, classical man-  
47 ual methods of analysis [7] allow to find in a suitable way 1D equilibrium solutions for the  
48 different types of vaults. The first research works on the numerical assessment of the static  
49 behavior of masonry vaults date back to the early 90s, see for instance the pioneering studies  
50 on the Brunelleschi Dome in [10]. As regards recently developed computational methods we  
51 can classify them into two broad categories [11]: (i) Thrust network methods, based on the  
52 Static Theorem of the limit analysis [12]-[16], and (ii) Finite and Discrete Element Methods,  
53 developed both for limit analysis and for nonlinear incremental analysis (see for instance  
54 FEM approaches in [17]-[24] and DEM approaches in [25]-[27]).

55 Concerning the studies published since 2000 it is possible to observe that a number  
56 of commercial software packages have been often used in the scientific literature to model  
57 masonry vaults. These programs are mostly FE codes developed to study concrete structures  
58 employing complex plastic-damaging constitutive models: cracks are taken into account as  
59 a kind of smeared distortions. The heterogeneity of masonry is not accounted for and  
60 isotropic behavior either in the elastic field or at collapse is generally assumed. However, it  
61 is worth noting that these techniques of analysis turn out to be adequate if combined with  
62 proper engineering reasoning. However, there is still much work to do on the definition of  
63 constitutive equations for masonry in the dynamic field. For example, with no claim to be  
64 exhaustive, the authors mention that: DIANA TNO [23] and NOSA CNUCE [24] contain  
65 specific software developed for studying masonry shells; [17] used ANSYS by assuming for  
66 masonry elastic-plastic material models (either Drucker-Prager or Willam-Wranke with low  
67 tension strength); [15] used Algor V21 with contact elements; [21] employed Abaqus by  
68 adopting a damage-plasticity approach.

69 However, only few of the cited papers are specifically addressed to the seismic analysis  
70 of masonry vaults. Moreover, they seem efficient for laboratory samples only, while the  
71 seismic behavior of historical masonry vaults strictly relies on the seismic response of the  
72 bearing structure. Accordingly, the numerical modeling of a historical masonry vault under  
73 earthquake actions cannot disregard the modeling of the bearing structure. Despite the  
74 problem importance, the role played by the structure on which the vaults rest has not been  
75 thoroughly studied.

76 With this in mind, this paper investigates the capabilities and **limitations** of current  
77 computational tools to simulate the seismic-induced damage in complex masonry vaulted  
78 structures. The case under study is the Giulio II vault, located in the main tower of the  
79 San Felice sul Panaro fortress (Italy) which has been severely damaged by the 2012 Emilia  
80 earthquake. The San Felice sul Panaro fortress has been subjected to several recent scientific  
81 studies. In particular, advanced FE mesh generation approaches have been proposed and  
82 applied to the fortress in [28, 29, 30, 31, 32]. Additionally, thorough numerical investigations  
83 on the seismic behavior of the main tower of the fortress have been carried out and some  
84 of the results are collected in [33, 34]. Particularly, the influence of adjacent buildings on  
85 the dynamic behavior of the main tower have been inspected in [34] where, in order to limit  
86 the computational effort, masonry vaults and timber floors have been modeled through  
87 equivalent plates (i.e. with the same in-plane stiffness), according to [3].

88 Here, the attention is focused on the modeling and analysis of the Giulio II vault and,  
89 particularly, on the interaction between the vault and its bearing system. The developed  
90 finite element model includes the 3D geometry of the vault within the geometry of the tower,  
91 based on a before-quake survey. Nonlinear static and dynamic analyses are carried out by  
92 using a damage-plasticity constitutive law. The results are compared to the vault actual  
93 crack pattern as well as to its actual-deformed geometry, based on a post-quake laser scanner  
94 survey.

95 The paper is organized as follows. Section 2 presents the case study, Section 3 illustrates  
96 the numerical modeling of the vault and Section 4 presents and discusses the numerical  
97 results, obtained by both nonlinear static and dynamic analyses. Concluding remarks end  
98 the paper (Section 5).

## 99 **2. Description of the case study**

100 The masonry vault which covers the Giulio II Hall in the main tower of the San Felice sul  
101 Panaro fortress (Figure 1), a town located near the city of Modena (Italy), is investigated.  
102 Such a cross vault (Figure 2) is located between the II and the III level of the main tower of  
103 the fortress (the tower on the right of Figure 1) and is characterized by an almost squared  
104 plan of approximately 6.5 meters, small ribs and a fresco (which portraits Saint Francis of  
105 Assisi) on its North side (Figure 2(c)). This latter artistic element further increases the  
106 heritage value of the case study, as commonly occurs for historical buildings [35, 36].

### 107 *2.1. Historical notes*

108 The San Felice sul Panaro fortress exhibits a very complex historical evolution along the  
109 centuries which also characterizes the Giulio II Hall's vault. Indeed, from the construction,  
110 which started in the XIV century, several alterations, modifications and reshuffles have taken  
111 place depending on the intended use changes of the parts of the monument. Consequently,  
112 the drafting of a very precise and accurate historical reconstruction of the evolution phases  
113 of the fortress, and in particular of the studied vault, was substantially impossible due to  
114 several lacks in the historical documents.



Figure 1: San Felice sul Panaro fortress.

115 Among the interesting documented events, it is worth noting that in 1511, when San  
 116 Felice sul Panaro town was involved in conflicts between the Houses of Pico, Pio and Este,  
 117 Pope Julius II (Giulio II in Italian) sojourned in the fortress and still nowadays there is  
 118 a room which bears his name (the Giulio II Hall). Indeed, for such an occasion a vaulted  
 119 room in the main tower of the fortress was prepared and two openings in the room, one as  
 120 a door (in the North side) and the other as a window (in the South side), were realized by  
 121 demolishing portions of the walls. Successively, one of the two aforementioned openings was  
 122 closed.

123 Another relevant event which characterizes the (more recent) history of the main tower  
 124 (and consequently of the Giulio II Hall's vault) consists of the construction, in 1920, of a  
 125 heavy cylindrical water reservoir made out of reinforced concrete in the IV level of the tower.  
 126 The cracking pattern appeared immediately after the first replenishment of the tank (which  
 127 principally consists in a sub-vertical crack from the V to the III level in the North side)  
 128 forced the emptying and later the complete dismantlement of the tank and the closing of  
 129 the cracks.

130 Among the more recent intended use of the Giulio II Hall, in 1999 the room was set  
 131 up for an archaeological exhibit as depicted in Figure 2(a) and Figure 2(b). In 2012 the  
 132 fortress, and consequently the Giulio II Hall's vault, was severely damaged by the Emilia  
 133 earthquake. The last arrangement of the Giulio II Hall before the earthquake is reported in  
 134 Figure 2(c). More details are reported in the following.

## 135 2.2. Emilia earthquake damage

136 During the second half of May 2012, the Emilia-Romagna region experienced a strong  
 137 seismic sequence which particularly damaged the historical architectural heritage of the  
 138 area [37, 38, 39]. In particular, the biggest quakes occurred within the provinces of Modena  
 139 and Ferrara. The main shocks have been recorded on May the 20th ( $M_w = 5.9$ ) and May

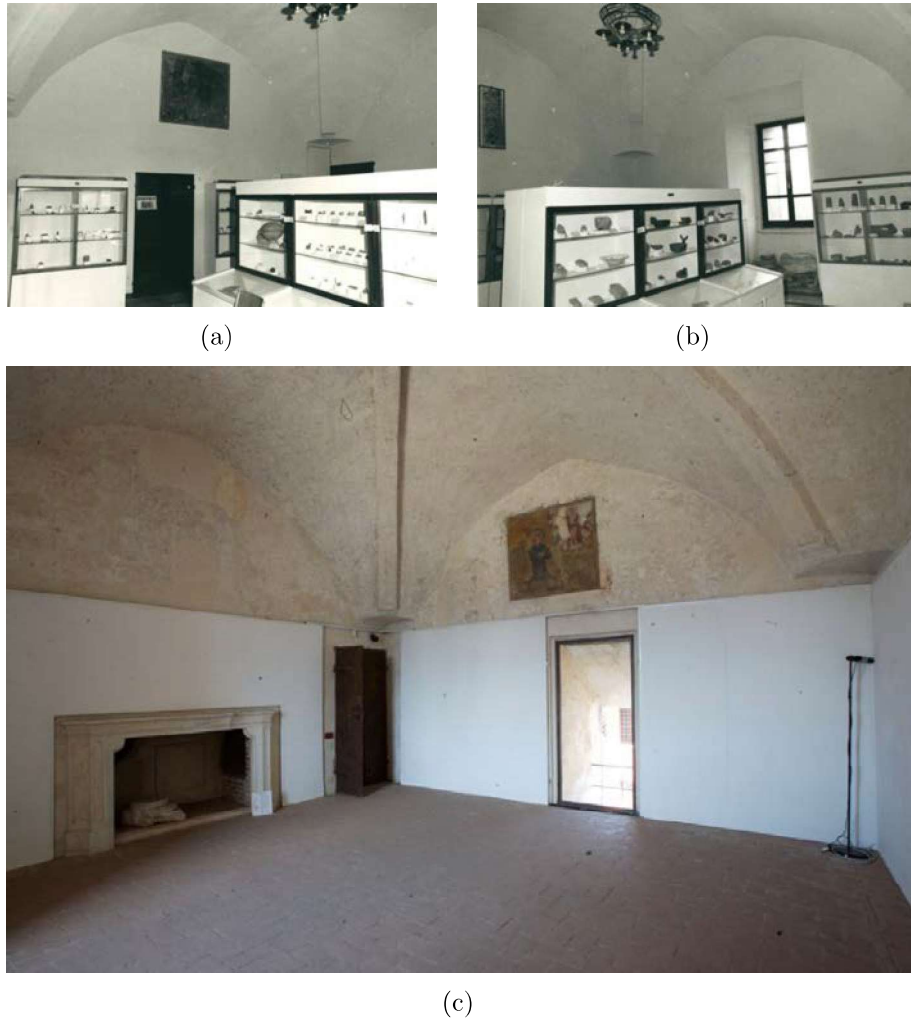


Figure 2: Giulio II Hall before the Emilia Earthquake.

140 the 29th ( $M_w = 5.8$ ) [40, 41], whose epicenters have been located at about 10 and 5 km from  
 141 San Felice sul Panaro, respectively [42]. An accurate outline of the damage experienced by  
 142 Emilian medieval fortresses due to the seismic sequence is reported in [43].

143 As a result, the fortress presented a widespread damage characterized by the collapse  
 144 of the crowning of the minor towers and the appearance of several deep cracks on the  
 145 main tower. In particular, the most relevant cracks appeared on the main tower consisted  
 146 in diagonal cracks, clearly visible in the lower half of the South (Figure 3(a)) and North  
 147 (Figure 3(b)) front. Approximately, these two main cracks are placed in the same plane,  
 148 roughly perpendicular to the line individuated by points H and L in Figure 3(c).

149 In the Giulio II Hall (whose position is highlighted by red frames in Figures 3(a) and  
 150 3(b) and by a blue dotted frame in Figure 3(c)), the vault which cover the room has been  
 151 interested by the presence of deep cracks and partial collapses, see Figures 4 and 5. In  
 152 general, it can be noted that the big flue chimney which is present inside the West wall of

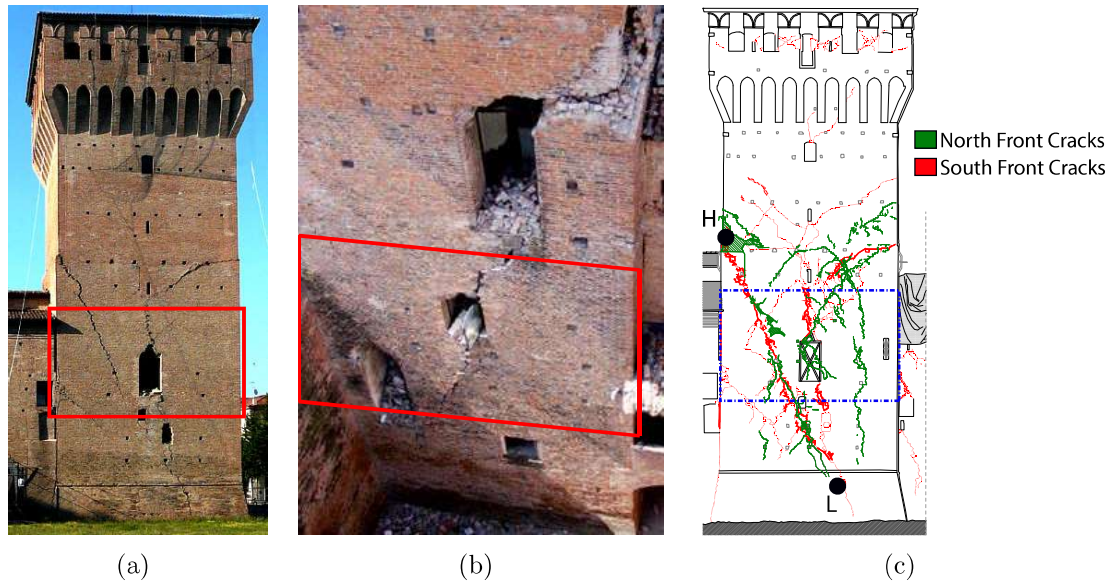


Figure 3: Main tower of San Felice sul Panaro fortress after the Emilia earthquake (2012): (a) Main tower's South front, (b) North front and (c) South and North fronts cracks superposition.

153 the tower could have weakened the masonry structure [43]. More specifically, by inspecting  
 154 Figure 4, the presence of four major failures of the vault, which are highlighted by the letters  
 155 a, b, c and d and are magnified in Figure 5, can be noted. In particular, by inspecting the  
 156 vault intrados the more severe damages can be summarized as follows:

- 157 (a) a collapse of a part of the vault near the flue chimney (West side), see Figure 5(a);
- 158 (b) a main and very severe crack which substantially cut in two parts the Giulio II Hall,  
 159 highlighted by blue arrows in Figure 4, see details in Figure 5(b);
- 160 (c) the detachment and collapse of the ribs, see Figure 5(c);
- 161 (d) a deep crack which starts from the upper extremity of the South-side-window, passes  
 162 near the vault's keystone and ends in the opposite side, see Figure 5(d).

163 The aforementioned damage pattern could be plausibly explained as follows:

- 164 • the partial collapse (a) could be due to the presence in **previous** times of an opening in  
 165 the vault for a stairwell inside the tower. Successively, due to the change of the tower's  
 166 intended use from defense purposes to residence the stair could have been removed  
 167 and the vault could have been closed. However, a discontinuity between the reshuffled  
 168 part and the original one due to a non-optimal tothing could have represented a  
 169 weakness zone during the seismic excitation leading to a local collapse. Moreover, the  
 170 aforementioned presence of the chimney hole in the West side could have weakened  
 171 the purpose of the bearing structure in such vault portion;



- 172 • the main crack (b) which passes through the vault along the N-S direction substantially  
173 links the two major diagonal cracks experienced by the main tower's South side (Figure  
174 3(a)) and North side (Figure 3(b)), as also shown in Figure 3(c);
- 175 • the detachment and collapse of the ribs (c) could be due to the fact that in this  
176 case the vault's ribs were added after the vault's construction. The role of the ribs  
177 in the mechanical behavior of masonry cross vaults has been the subject of intense  
178 debates since the 19th century [9, 44] and numerical analyses have been employed to  
179 investigate their effects [45]. However, the hypothesis of later decorative non-structural  
180 ribs is made by the authors due to the presence of an almost regular layer of a relatively  
181 recent cementitious mortar between the ribs and the vault (Figure 5(c)).
- 182 • the crack (d) starts from the window in the South side of the tower (Figure 5(d)).  
183 Such an opening was obtained by demolishing a portion of the wall, as said before.  
184 This fact, as well as the absence of an adequate lintel over the opening, could have  
185 weakened this part of the structure.

186 Summing up, it emerges that the damages experienced by the vaulted structure during  
187 the earthquake are strictly linked to its historical evolution phases (e.g. failures (a), (c)  
188 and (d) in Figures 4 and 5) and to the seismic-induced damage experienced by the masonry  
189 tower, i.e. the vault's bearing structure (e.g. failure (b) in Figures 4 and 5).

190 Finally, it has also to be pointed out that the perimeter wall of the East side of the  
191 Giulio II Hall detached from the floor of approximately 6 centimeters (Figure 6), while in  
192 the other sides no relevant detachments appeared.

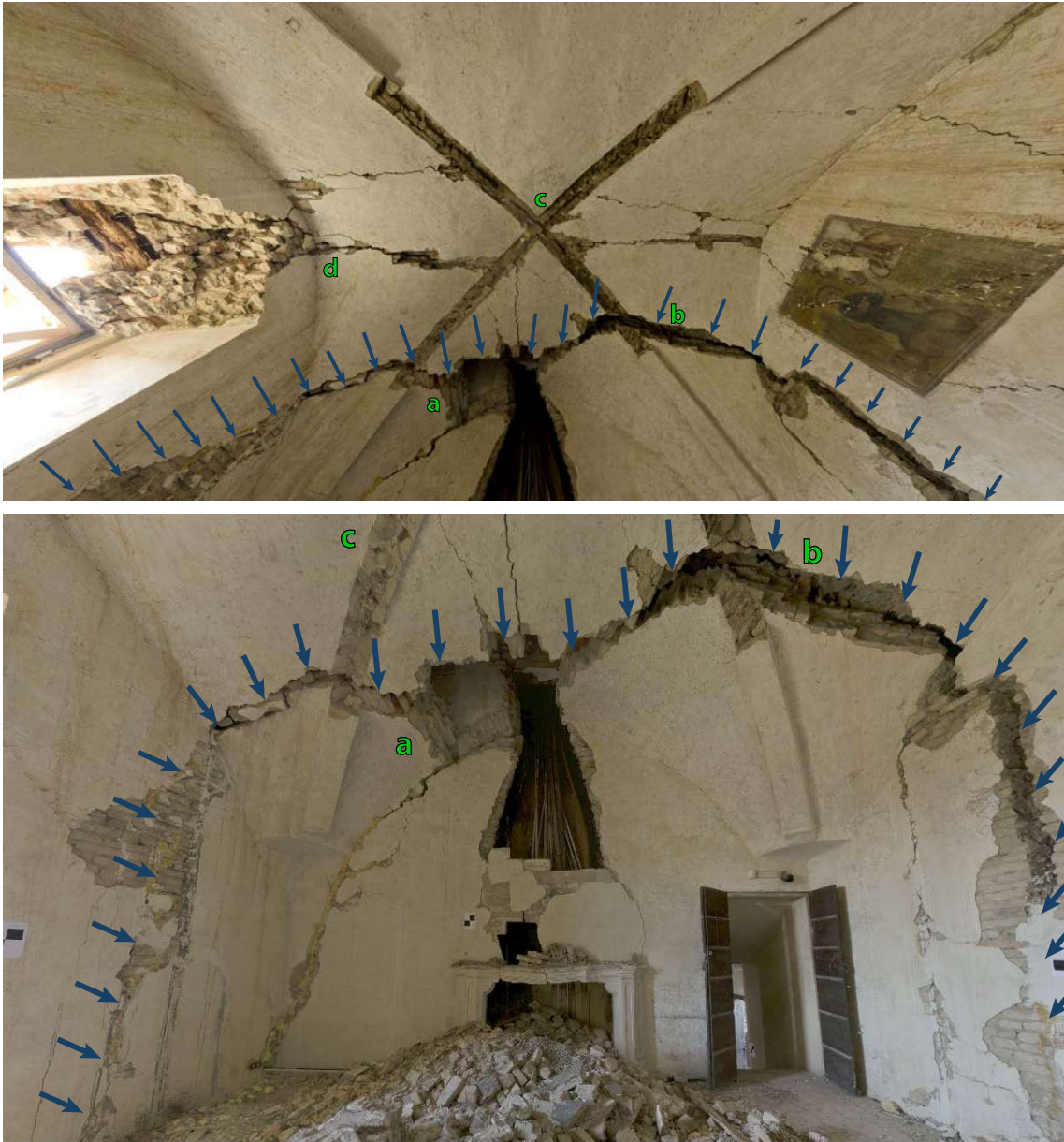
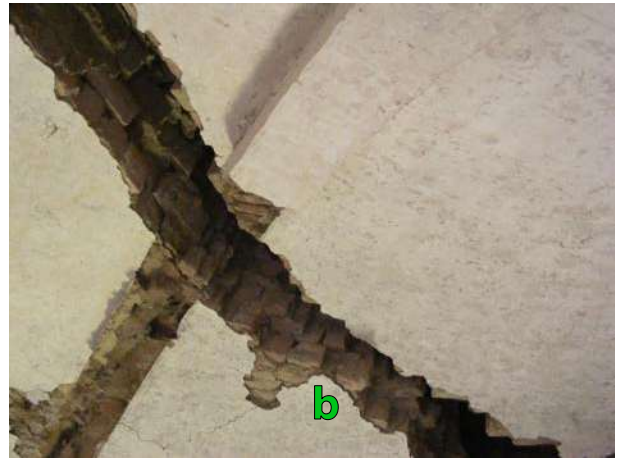


Figure 4: Giulio II Hall's vault after the Emilia earthquake.



(a)



(b)



(c)



(d)

Figure 5: Giulio II Hall's vault major failures. The letters a, b, c and d are referred to Figure 4.

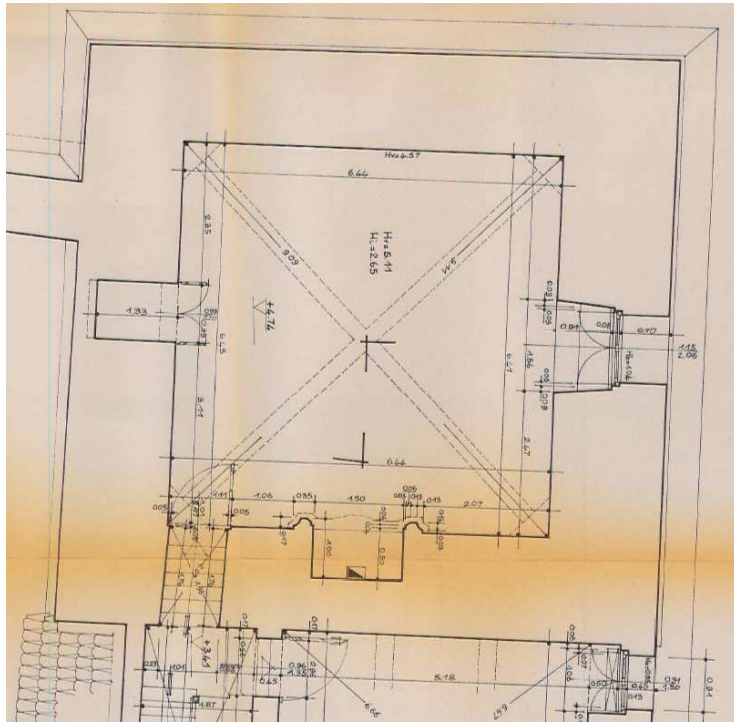


Figure 6: Detachment between the floor and the East wall of the Giulio II Hall after the Emilia earthquake.

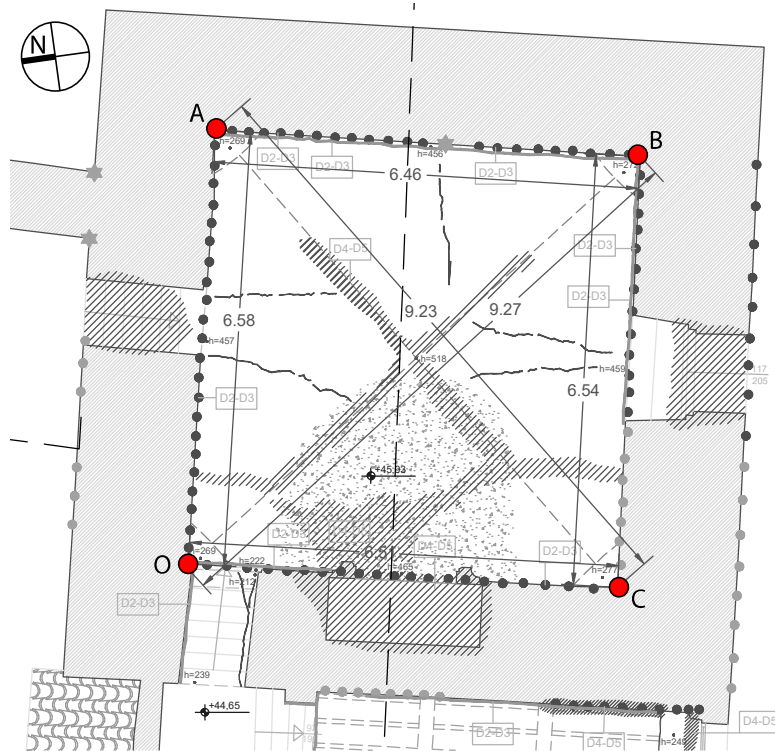
193 *2.3. Vault surveys*

194 Aiming at quantitatively assessing the effects of the seismic action on the vault, a com-  
195 parison between two different surveys, one made in 1985 (the only available before the  
196 earthquake) and one made in 2012 after the earthquake, has been carried out in terms of  
197 vault's abutments relative displacements. However, it has to be pointed out that the two  
198 geometrical surveys were conducted in different times with completely different techniques  
199 characterized by different accuracy. In particular, the first one was performed in 1985 with  
200 classical hand-based survey procedure, whereas the second one was carried out in 2012 with  
201 the laser scanner technique. Coarsely, if the first one guarantees the accuracy of some cen-  
202 timeters, the second one guarantees the accuracy of some millimeters. The comparison of  
203 the Giulio II Hall's vault plan before and after the seismic event is reported in Figure 7, while  
204 the comparison of its N-S section and its E-W section is reported in Figure 8. Concerning  
205 Figure 7, it should be noted that it is not precisely known at what height the plan of Figure  
206 7(a) (1985 survey) is taken (there is about 1 m of uncertainty).

207 The resulting actual relative displacements of the vault's abutments measured between  
208 the plan of Figure 7(a) and the plan of Figure 7(b) are collected in Table 1. The letters  
209 O, A, B and C are referred to Figure 7(b). As can be noticed in Table 1, relevant relative  
210 displacements have been recorded: the two diagonals of the vault (OB and CA) measure an  
211 increase of length of more than 14 cm; the sides along the E-W direction measure an increase  
212 of length of 13 cm (OA and BC) whereas the sides along the N-S direction presented shorter  
213 relative displacements of 7 (CO side) and 2 cm (AB side). Due to the different nature of the  
214 two compared surveys, the quantities collected in Table 1 have to be considered as affected by  
215 some uncertainties of the order of magnitude of centimeters. No other experimental findings  
216 are available for the Giulio II Hall's vault (in terms, for instance, of endoscope tests) since its  
217 compromised safety condition did not permit any experimental test. Therefore, no detailed  
218 information of the stratigraphy of the vault are available. However, by visually inspecting  
219 the vault's deep cracks, the assumption of 42 cm thickness has been made.

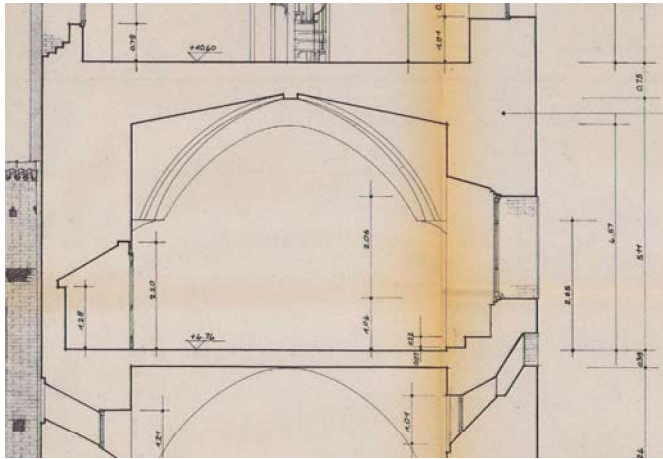


(a)

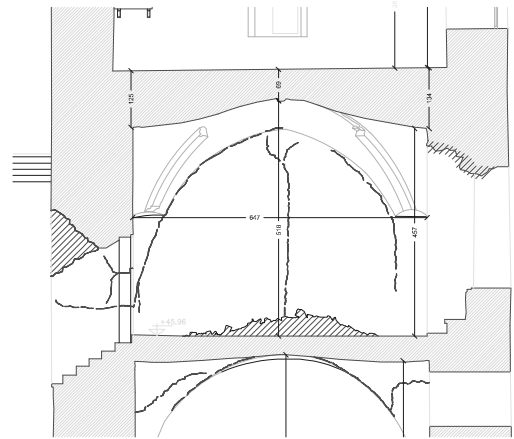


(b)

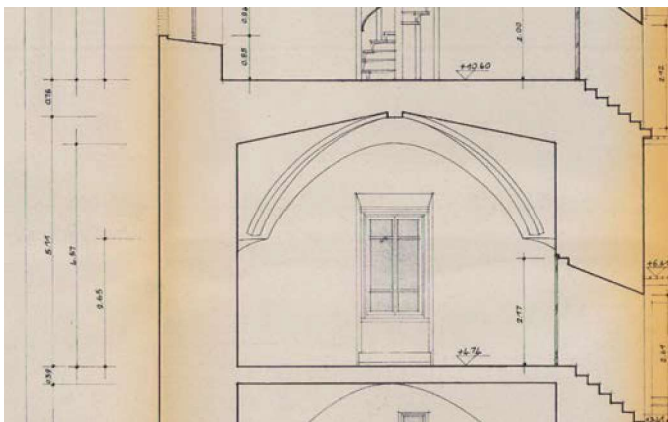
Figure 7: Giulio II Hall's vault plan: (a) before the earthquake (1985 survey) and (b) after the earthquake (2012 laser scanner survey).



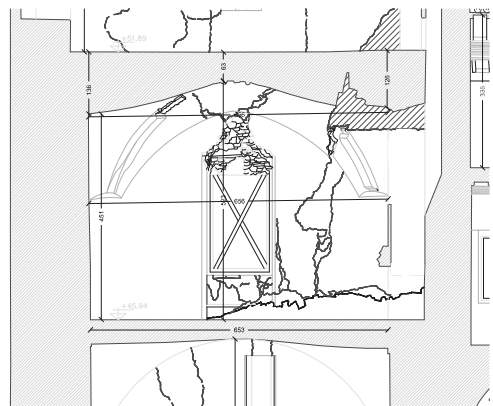
(a)



(b)



(c)



(d)

Figure 8: Giulio II Hall's vault sections: N-S section (a) before (1985 survey) and (b) after the earthquake (2012 laser scanner survey), E-W section (c) before and (d) after the earthquake.

Table 1: Relative displacements of the vault’s abutments according to the measurements made before and after the earthquake, see Figure 7.

Vault’s side	1985 survey	2012 survey	Rel. displ.
OA	645 cm	658 cm	13 cm
AB	644 cm	646 cm	2 cm
BC	641 cm	654 cm	13 cm
CO	644 cm	651 cm	7 cm
OB	911 cm	927 cm	16 cm
CA	909 cm	923 cm	14 cm

### 220 3. Numerical modeling

221 The numerical modeling of the case-study has been carried out through a 3D FE model.  
 222 The geometry has been obtained through a 3D CAD modeling, based on the 1985’s survey  
 223 (before earthquake). As anticipated, the vault 3D FE model is included within the 3D FE  
 224 model of the tower having, hence, a unique detailed model. This choice is crucial in order  
 225 to investigate how the seismic behavior of the tower influences the seismic-induced damage  
 226 of secondary elements such as vaults, given their mutual and direct interaction.

227 Based on the vault’s survey, the following assumptions in the numerical modeling of the  
 228 vault are made:

- 229 (i) absence of ribs, since they appear to have only a decorative function, see Figure 5(c);
- 230 (ii) vault without any hole, to model the vault condition before the earthquake;
- 231 (iii) equivalent masses have been applied on the vault in order to take into account the infill  
 232 weight, made up of a heterogeneous material, and the pavement.

233 The 3D FE mesh of the tower, which includes the vault, is depicted in Figure 9. Hori-  
 234 zontal axes of the model (X and Y) substantially correspond to the cardinal directions (S-N  
 235 and E-W, respectively). In order to maintain acceptable the computational cost, the mesh  
 236 design aimed at guaranteeing a fine description of the vault and a coarser description of the  
 237 tower. In any case, the presence of at least three tetrahedron elements on the thickness of  
 238 the tower trunk’s walls (Figure 9(c)) guarantees a reasonable accuracy in terms of global  
 239 structural behavior of the tower. The adopted FE mesh counts 20,393 nodes and 79,459  
 240 tetrahedron elements.

241 As extensively discussed in [34], the seismic behavior of the tower is influenced by the  
 242 presence of adjacent structural elements. Therefore, some portions of the adjacent buildings  
 243 have been considered in the FE model (Figure 9(a)). Therefore, in order to approximately  
 244 take into consideration the stiffness of the non-meshed parts of the fortress while keeping  
 245 simple the model and low the computational effort, rollers have been inserted on the surfaces  
 246 highlighted by purple arrows, see Figure 9(a).

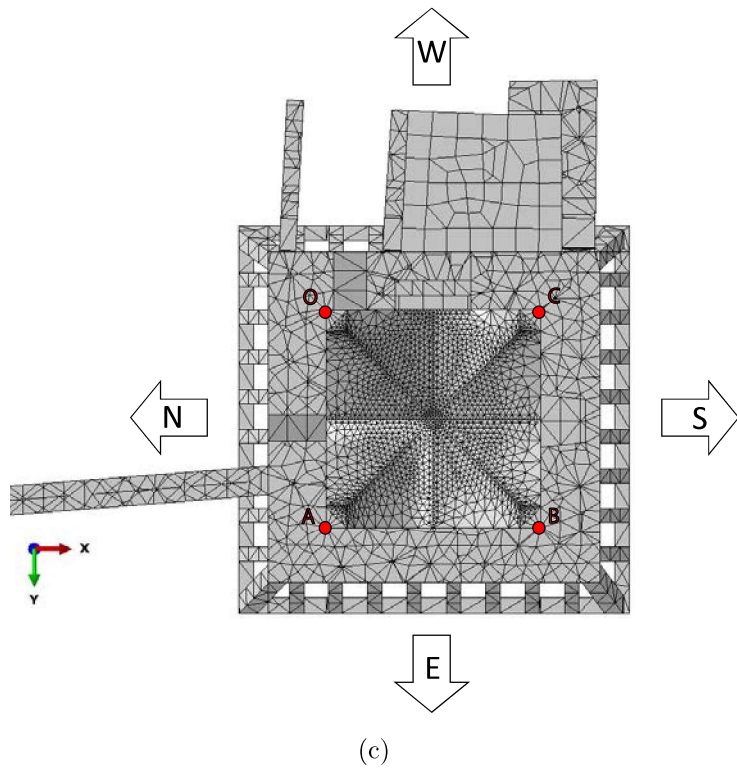
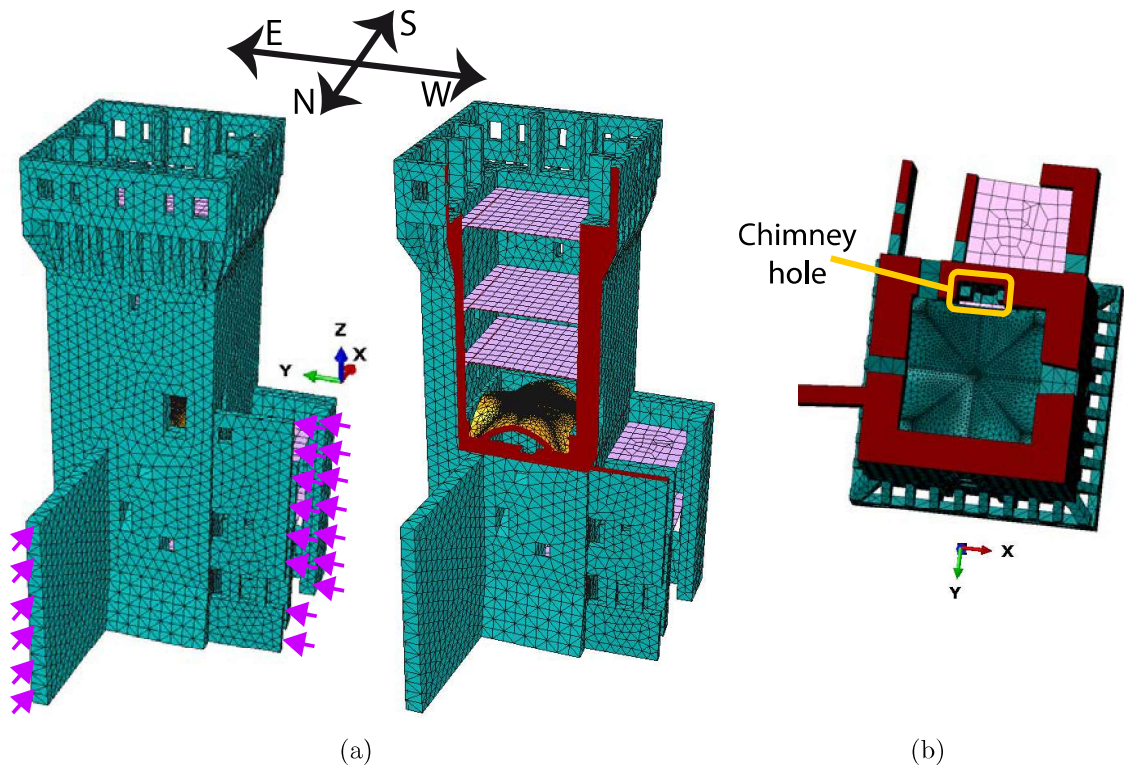


Figure 9: Vault and the tower's 3D FE numerical modeling: (a) 3D FE mesh, (b) particular of the chimney hole and (c) Giulio II Hall's vault mesh with the considered points of the model, bottom view.



247 *3.1. Constitutive model for masonry*

248 The implementation of constitutive models able to simulate the mechanical behavior of  
 249 masonry is a challenging task, especially in dynamic simulations. Masonry is characterized  
 250 by an orthotropic behavior, both in the linear and nonlinear fields [46]. Interesting progresses  
 251 have been achieved in masonry orthotropic damage models [47], even if their application to  
 252 3D large-scale problems appears inefficient due to their high computational demand and,  
 253 hence, their limitation to small-scale structures. For this reason, the use of isotropic damage  
 254 models for full-scale masonry structures is commonly accepted [29]. **In particular, the case  
 255 study presents very thick walls with a chaotic masonry texture, for which a orthotropic  
 256 model appears as questionable as an isotropic one.**

257 In this paper, isotropic material behavior has been assumed and the Concrete Damage  
 258 Plasticity (CDP) model, available within the Abaqus software [48], has been used to perform  
 259 nonlinear static and dynamic analyses. Even though such a model has been designed for  
 260 concrete, the authors experienced successful results for masonry structures, see for instance  
 261 [29, 34]. The material properties as well as the model parameters used in numerical analyses  
 262 are collected in Table 2. In the following, the main model parameters are briefly discussed.  
 263 The interested reader is referred to [48, 29] for more details.

Table 2: Material properties and model parameters used in numerical analyses.

Material properties and parameters		Values	
Young's modulus $E_0$ [MPa]		1500	
Poisson's ratio		0.2	
Dilatation angle		10	
Eccentricity		0.1	
$f_{b0}/f_{c0}$		1.16	
$K_c$		2/3	
Viscosity Parameter		0.002	
Tensile mono-axial curve		Compression mono-axial curve	
Stress [MPa]	Inelastic strain	Stress [MPa]	Inelastic strain
0.12	0	2.0	0
0.0012	0.001	2.4	0.002
0.0012	0.003	0.2	0.007

264 The CDP model uses a Drucker-Prager strength criterion, modified through a parameter,  
 265  $K_c$ , which represents the ratio between the distance from the hydrostatic axis of the maxi-  
 266 mum compression and tensile stress [48, 49, 50]. Furthermore, the CDP model considers **an**  
 267 eccentricity parameter, which serves to regularize the tensile corner, and a nonassociated po-  
 268 tential flow rule for the elasto-plastic deformation part. Such a feature gives the possibility  
 269 to account for the dilatance phenomenon, governed by the dilatation angle, **which has been**  
 270 **assumed equal to 10 degrees** [51, 52]. The ratio between the bi-axial,  $f_{b0}$ , and mono-axial,  
 271  $f_{c0}$ , compression strength has been supposed according to [46]. In order to better ensure the  
 272 algorithm convergence in the nonlinear range, viscoplastic regularization is implemented and

273 is defined through a viscosity parameter, assumed in agreement with the outcomes emerged  
274 in [29].

The damage effects consist in the gradually reduction of the Young's modulus every time the strain reaches a critical value. The following standard relationships define the mono-axial tensile  $\sigma_t$  and compressive  $\sigma_c$  stresses:

$$\sigma_t = (1 - d_t)E_0(\varepsilon_t - \varepsilon_t^{pl})$$

$$\sigma_c = (1 - d_c)E_0(\varepsilon_c - \varepsilon_c^{pl})$$

275 where  $E_0$  is the initial elastic modulus,  $d_t$  and  $d_c$  are the scalar damage variables in tension  
276 and in compression,  $\varepsilon_t$  and  $\varepsilon_c$  are the total strain in tension and in compression,  $\varepsilon_t^{pl}$  and  $\varepsilon_c^{pl}$   
277 are the equivalent plastic strain in tension and in compression. In addition, such a constitutive  
278 model accounts for the effect of closing of previously formed cracks under dynamic loading  
279 conditions, which results in the recovery of the compression stiffness.

280 **The choice of mechanical properties for historical masonry is a challenging task. The**  
281 **availability of extensive destructive and non-destructive in situ tests should help the analyst**  
282 **in calibrating the mechanical model. However, such tests are generally expensive and inva-**  
283 **sive. Furthermore, their reliability for historical buildings is reduced due to the irregularities**  
284 **which characterize such structures.**

285 No comprehensive results of experimental tests were available for the case study and,  
286 aiming at defining the material mechanical properties, it was essential to refer to national  
287 codes for existing buildings [54, 55, 56]. Material properties have been assumed considering  
288 the lowest level of knowledge (the so-called LC1 in [54]) and a clay bricks masonry with  
289 very poor mortar and quite regular texture. In addition, tensile and compression mono-  
290 axial curves (see Table 2) have been implemented according to [53], where the numerical  
291 investigations of two coeval case studies of similar masonry towers, located approximately  
292 at 10 km far from the case study under consideration, have been presented. Indeed, it is  
293 worthy to point out that medieval buildings in the area stricken by the 2012 seismic sequence  
294 exhibited a quite similar masonry strength [57]. Finally, a linear reduction until 90% of the  
295 Young's modulus with respect to  $E_0$  for an inelastic deformation equal to the lower extremity  
296 of compressive and tensile softening branches (Table 2) has been assumed.

#### 297 **4. Numerical analyses**

298 In order to investigate the seismic-induced damage in the considered historical cross  
299 vault, nonlinear static and dynamic analyses are performed on the 3D FE model depicted  
300 in Figure 9. The analyses are especially focused on the mutual interaction between the  
301 tower and the vault and, hence, particular attention is devoted to the vault abutments  
302 displacements. Figure 9(c) shows the considered points of the vault abutments used to  
303 compute displacements in the following analyses.

#### 304 4.1. Nonlinear static analyses

305 Nonlinear static analyses have been performed by applying along the tower's principal  
306 axes horizontal forces derived by the assumption of a linear variation of acceleration along  
307 the height (called G1 in [54]). This distribution is, generally, the most critical for such kind  
308 of structures [52]. Such analyses are pushed over a drop of 20% of the base shear of the  
309 tower.

310 Figures 10, 11, 12 and 13 illustrate the base shear-vault abutments displacements curves  
311 for the East, West, South and North load cases, respectively. On one hand, in the East  
312 (Figure 10) and South (Figure 12) load cases the vault's abutments tend to significantly  
313 distance themselves. In particular, points belonging to the side which is pushed outwards  
314 (i.e. A and B for the East load case and B and C for the South load case) show larger  
315 displacement than the others of the same load case. Furthermore, points belonging to the  
316 same side perpendicular to the force direction record similar displacement in this two load  
317 cases. On the other hand, the West load case (Figure 11) shows a quasi-linear behavior  
318 and, also after the failure of the tower, the relative displacements of the abutments are  
319 considerably lower than the other load cases. As can be particularly noted in Figure 11, the  
320 displacements at null base shear are different from zero. This is due the fact that before  
321 pushing the structure horizontally, the model is subjected to a vertical gravitational load  
322 which produces slight horizontal displacements of the vault abutments. Finally, concerning  
323 the North load case (Figure 13), it appears that Point O's displacement is clearly larger than  
324 Point A's one, although they belong to the same side perpendicular to the horizontal force,  
325 highlighting a torsion of the tower. This phenomenon could be addressed to the presence of  
326 the curtain wall in the North side, as further discussed in the following.

327 Summing up the results, Figure 14 illustrates the base shear-relative displacements curves  
328 between the points which belong to vault sides parallel to the applied force. It is worth-  
329 noting that for the East directed force the abutments tend to distance themselves for base  
330 shear values slightly lower than the other cases. In addition, both the load cases East and  
331 South show similar relative displacement between the two sides parallel to the applied force  
332 for each analysis (i.e. between AO and BC and between CO and BA). In particular, in the  
333 East load case the side AO gains distance earlier than side BC, plausibly due to the fact  
334 that the North side of the tower presents three almost aligned openings (see Figure 9) which  
335 reduce the capacity of the structure's side. Furthermore, concerning the North load case it  
336 can be noted that, as already mentioned before, the side OC records relative displacement  
337 considerably greater than the other side AB. This effect could be reasonably addressed to  
338 the presence of the curtain wall in the North side of the tower (see Figure 9(a)) which  
339 acts as a North directed displacement constraint and limits the abutment A displacements.  
340 Finally, in the West load case the effect of the constraint offered by the tower's adjacent  
341 building in the West side (Figure 1) is essential and consists in a substantial limitation of the  
342 absolute displacement of the vault abutments. In particular, such a constraint almost exactly  
343 acts until the height of the vault abutments, see Figure 9. Consequently, the abutments'  
344 displacements are considerably limited (Figure 11). Moreover, the constraint offered by the  
345 adjacent building is overall uniform and no significant torsion of the tower is recorded, see  
346 Figure 14.

347 Table 3 collects the relative displacements of the vault's abutments at the ultimate  
348 displacement of the tower, i.e. when the base shear shows a drop of 20%. Such displacements  
349 are also highlighted on the curves of Figure 14 through a hexagon. As can be noted, the East  
350 and South load cases show greater relative displacements at the ultimate condition than the  
351 other load cases (included between 5.8 and 7.4 cm). This fact could also be addressed to  
352 the presence of adjacent structural elements in the other directions.

353 In Figures 15, 16, 17 and 18, damage contour plots of the four load cases (East, West,  
354 South and North, respectively) are reported for three subsequent simulation instants. In  
355 particular, in order to compare the evolution of the damage for each analysis these plots  
356 have been taken (a) at a step right after leaving the linear regime, (b) at an intermediate  
357 step between the first instant and the ultimate condition and (c) at the ultimate condition  
358 of the tower.

359 Concerning the East load case, the damage contour plots (Figure 15) show the develop-  
360 ment of a crack in the intrados which is perpendicular to the East direction. In particular,  
361 the development of this crack is already clear at the first considered instant, see Figure 15(a).  
362 In addition, such a crack is in good agreement with the actual crack pattern experienced  
363 by the vault, for instance compare Figure 15(b) with Figure 4 (failure (b)). Furthermore,  
364 from the second instant on out it appears a crack perpendicular to the East direction also in  
365 the vault extrados, see the section view of Figures 15(b) and 15(c). Although no reference  
366 is available for the vault extrados actual crack pattern, by inspecting Figure 6 it clearly  
367 appears that the main crack (b) crosses the whole thickness of the vault.

368 As far as the West directed force analysis is concerned, the strong interaction with the  
369 adjacent building, which deeply limits the structure displacements along the West direction,  
370 restricts the damage in the higher part of the tower's trunk and no significant cracks appear  
371 in the vault (Figure 16).

372 For what concern the South load case, as already noted in Figure 14, the points of the  
373 sides parallel to the force direction tend to distance themselves in a similar way. This is also  
374 confirmed by the damage contour plots of Figure 17 which show the progressive development  
375 of a crack in the intrados perpendicular to the South direction.

376 Concerning the North load case, due to the strong interaction with the curtain wall, the  
377 torsion of the tower is recorded (as reported in Figure 14) and the damage pattern of the  
378 vault (Figure 18) is conditioned by this effect. Indeed, in the vault intrados it emerges a  
379 crack which approximately tends to link the contact point with the curtain wall and the  
380 point C (Figure 9(c)) of the vault, see the progression of such a crack in Figure 18. This  
381 crack is in agreement with the actual crack specular to the failure (d) in Figure 4.

382 Summing up, nonlinear static analyses seem to be qualitatively able to investigate the  
383 main weaknesses of the vault.

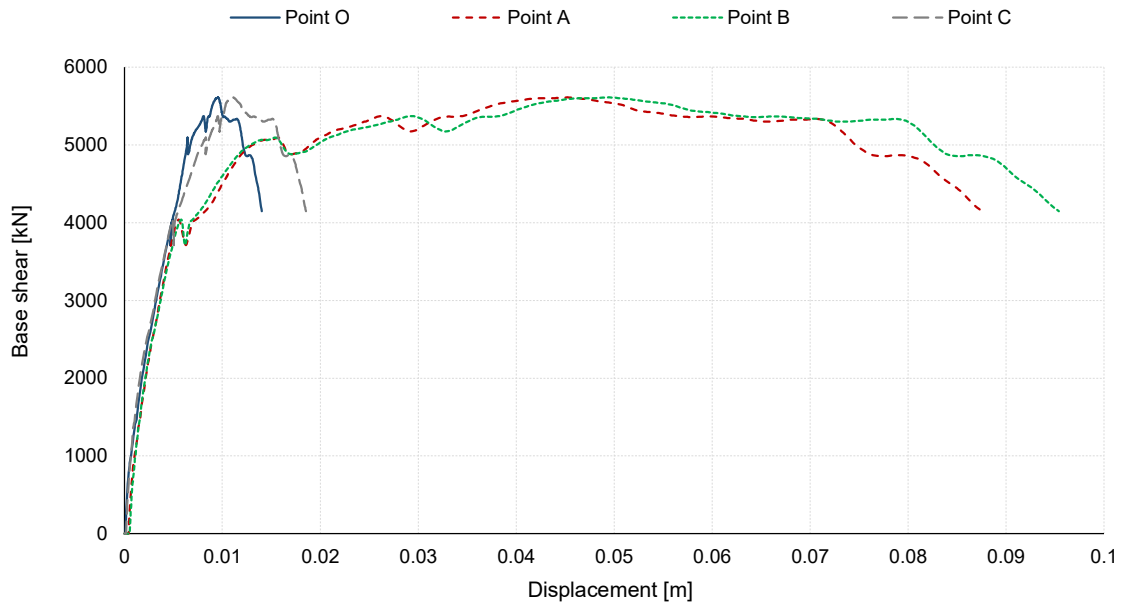


Figure 10: Base shear-displacement of the vault's abutments curve of the points depicted in Figure 9(c), East directed force.

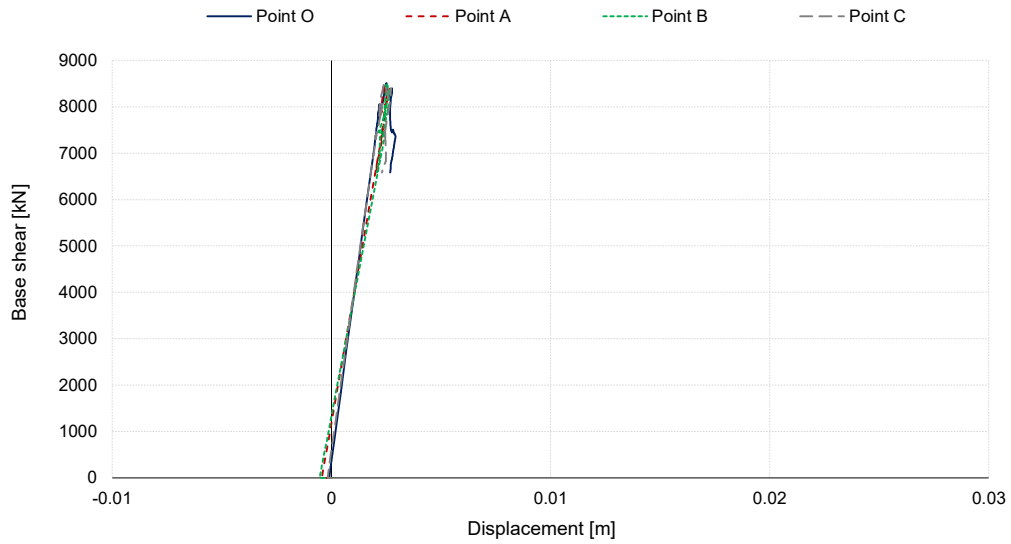


Figure 11: Base shear-displacement of the vault's abutments curve of the points depicted in Figure 9(c), West directed force.

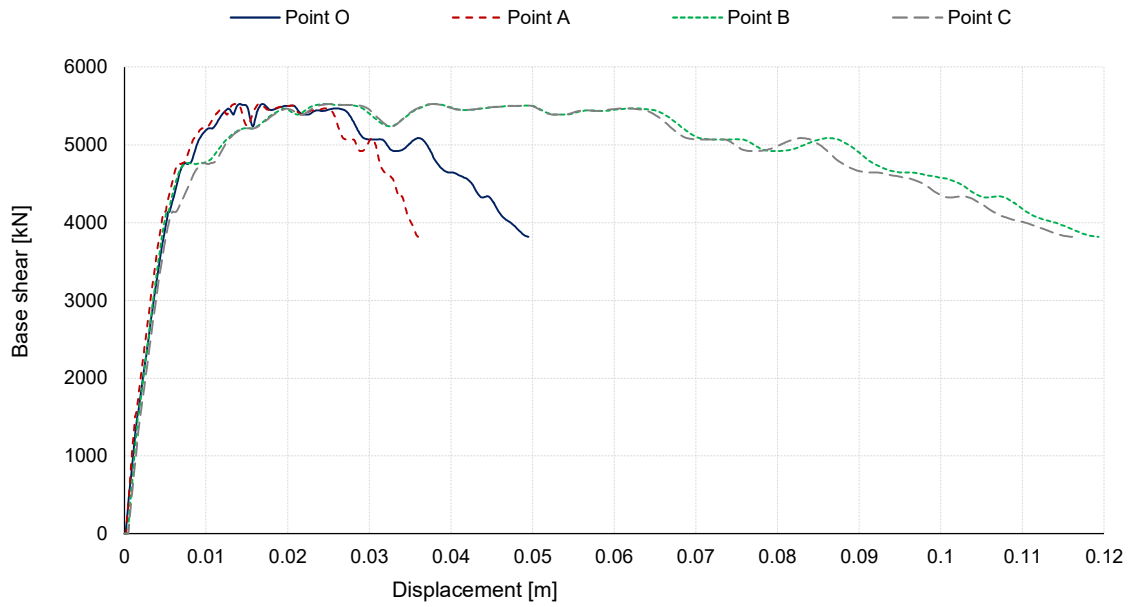


Figure 12: Base shear-displacement of the vault's abutments curve of the points depicted in Figure 9(c), South directed force.

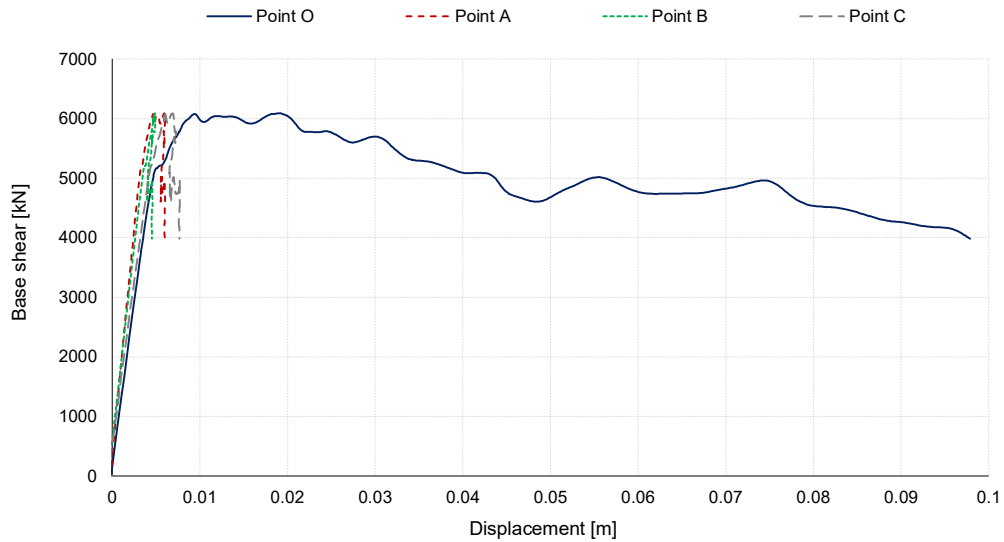


Figure 13: Base shear-displacement of the vault's abutments curve of the points depicted in Figure 9(c), North directed force.

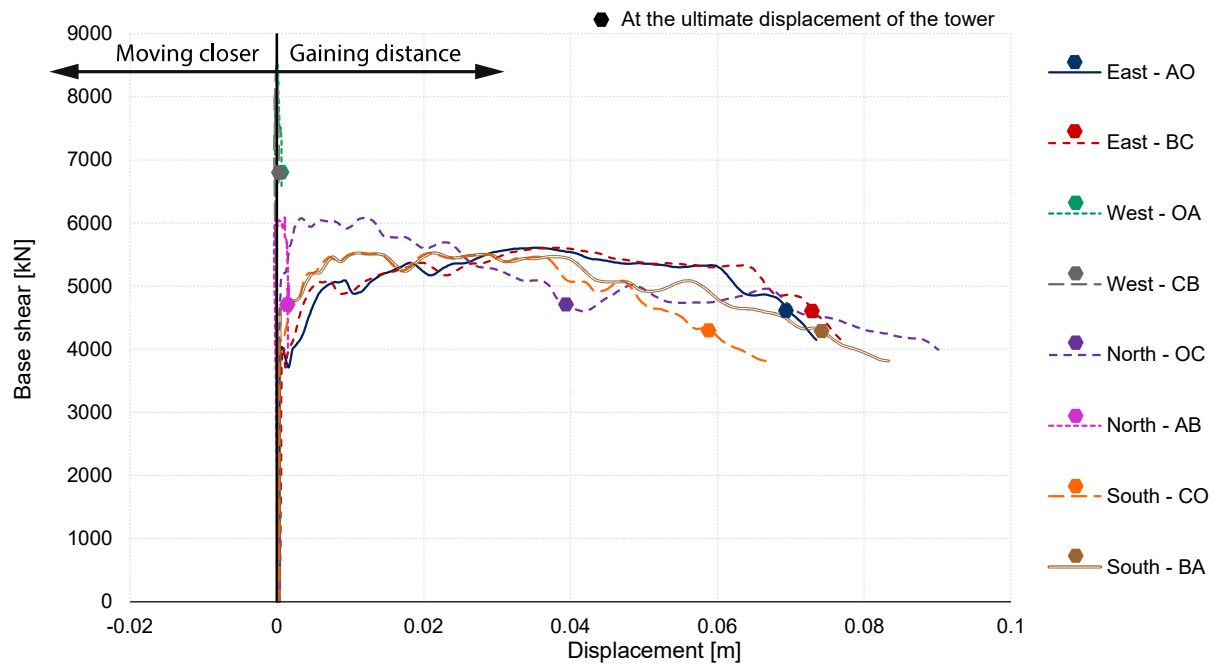


Figure 14: Base shear-relative displacement of the vault's abutments curves between the points depicted in Figure 9(c).

Table 3: Relative displacements of the vault's abutments at the ultimate displacement of the tower.

Direction	Side	Relative displacement
E	$\Delta AO$	6.9 cm
E	$\Delta BC$	7.3 cm
W	$\Delta OA$	0.1 cm
W	$\Delta CB$	0.1 cm
N	$\Delta OC$	3.9 cm
N	$\Delta AB$	0.2 cm
S	$\Delta CO$	5.8 cm
S	$\Delta BA$	7.4 cm

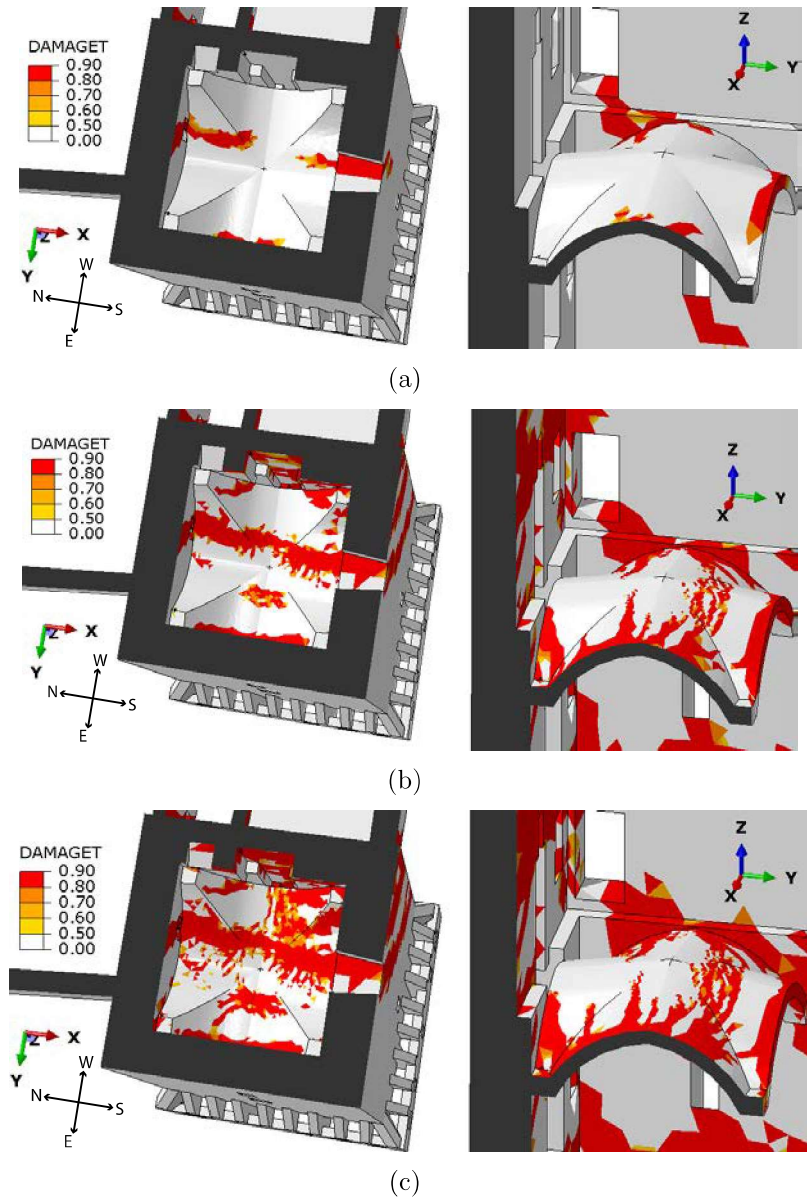


Figure 15: Nonlinear static damage contour plots of the Giulio II Hall's vault, East directed force. Bottom views (left) and section views (right).



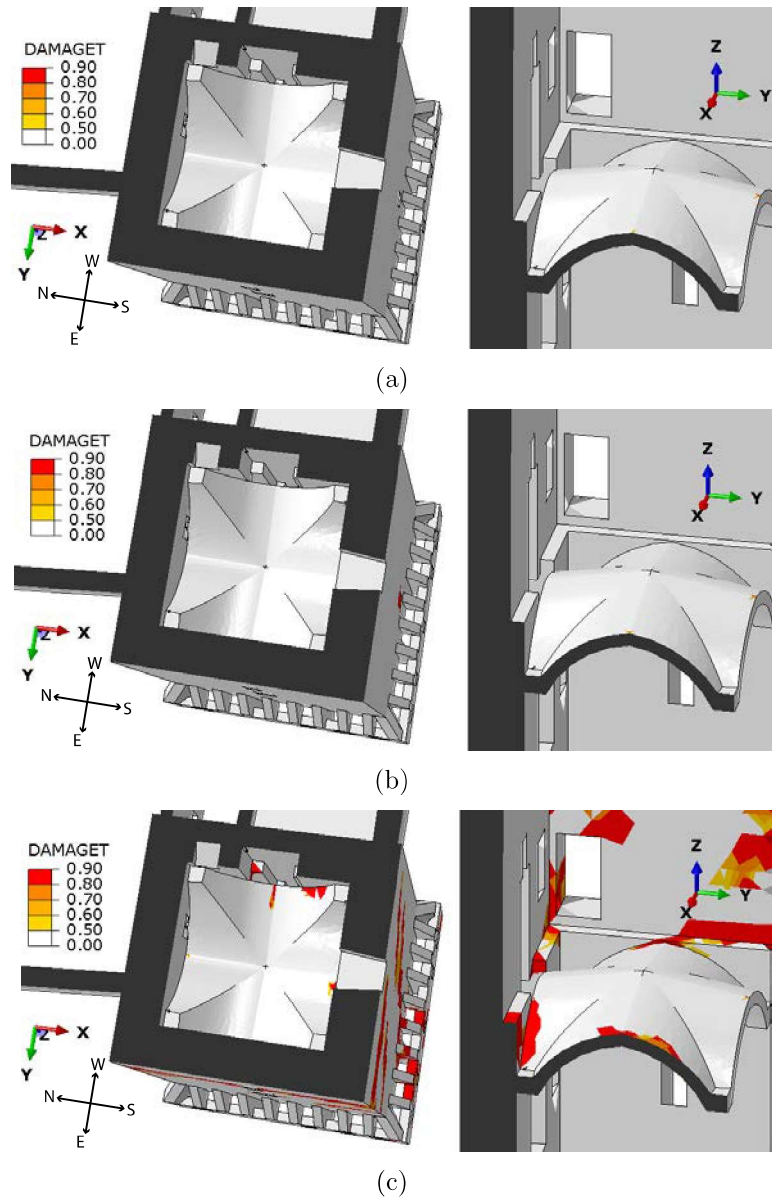


Figure 16: Nonlinear static damage contour plots of the Giulio II Hall's vault, West directed force. Bottom views (left) and section views (right).

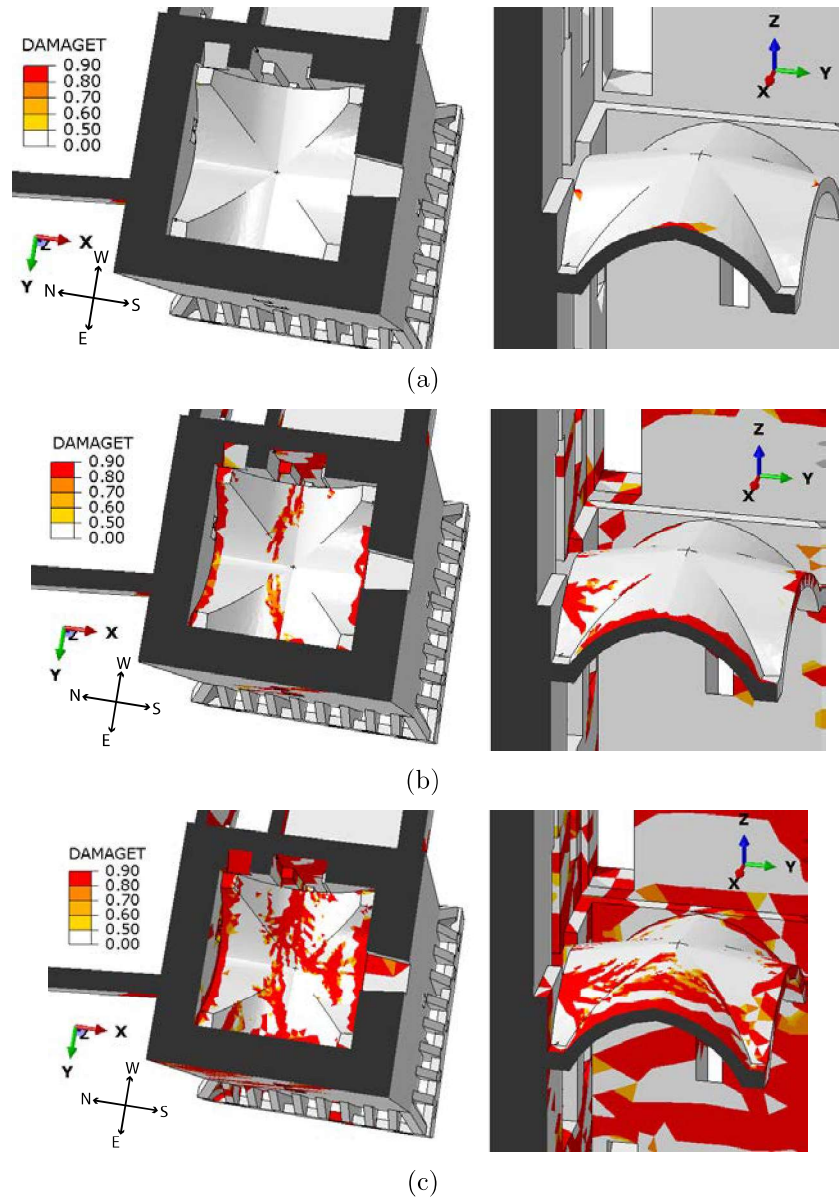


Figure 17: Nonlinear static damage contour plots of the Giulio II Hall's vault, South directed force. Bottom views (left) and section views (right).

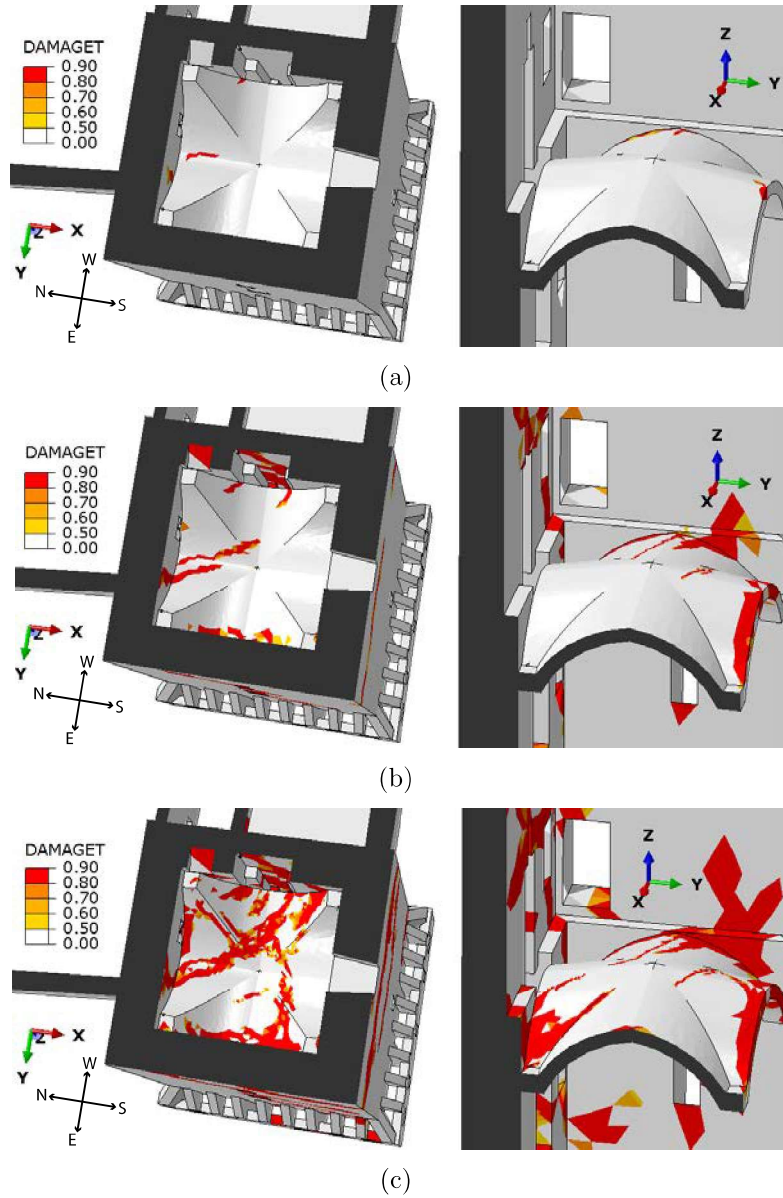


Figure 18: Nonlinear static damage contour plots of the Giulio II Hall's vault, North directed force. Bottom views (left) and section views (right).

384 *4.2. Nonlinear dynamic analyses*

385 Nonlinear dynamic analyses have been performed using the only actual accelerogram  
 386 available near to the fortress, recorded on May 29th at the *SANO* station (installed after the  
 387 first seismic shock [40, 41]) located at approximately 150 m from the fortress. In particular,  
 388 11-seconds simulations have been performed by considering either the horizontal components  
 389 only or also the vertical component of the accelerogram [42], see Figure 19.

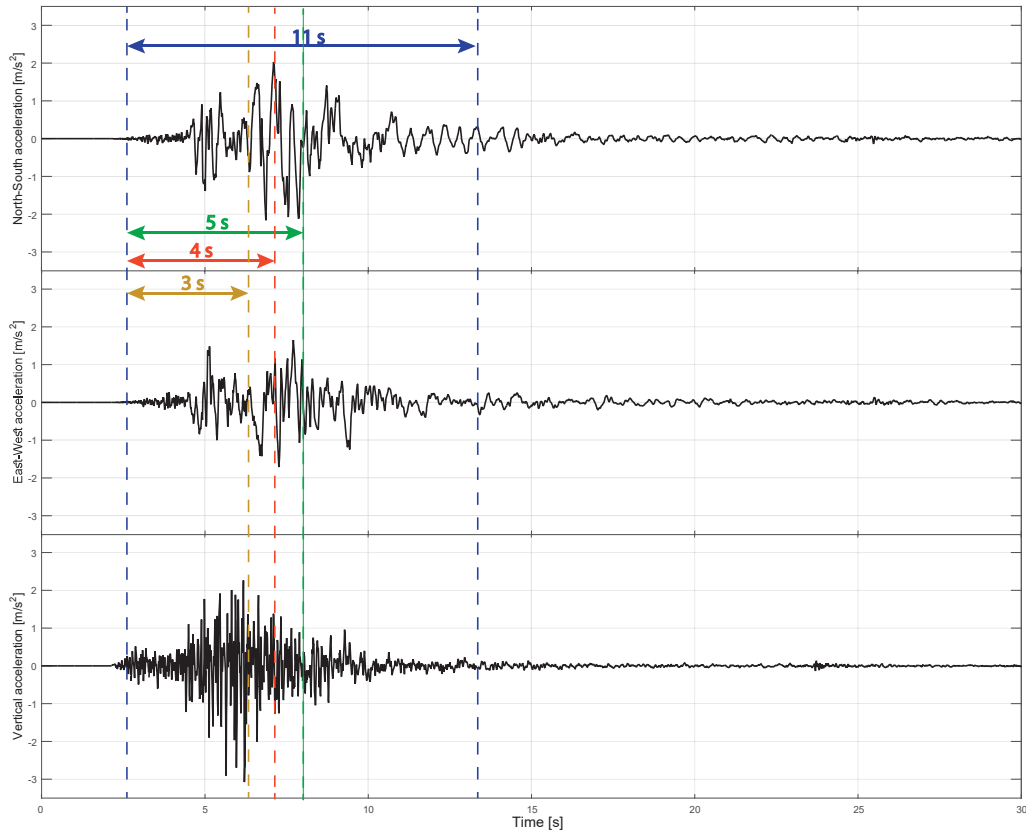


Figure 19: Accelerograms recorded the May 29th 2012 at *SANO* station.

390 It is well-known that the dynamic structural response is significantly conditioned by the  
 391 damping. However, the implementation of damping models for masonry structures in the  
 392 inelastic regime is still a challenging issue. In dynamic simulations, a Rayleigh damping  
 393 model has been used, as adopted for masonry structures in [58, 59].

394 The time-histories of the Giulio II Hall's vault abutments relative displacements are  
 395 reported in Figure 20 (computed with respect to the point O, see Figure 9(c)). As can  
 396 be observed in Figure 20, the time-histories of the relative displacements of the vault's  
 397 abutments of the case without vertical component of the earthquake (Figure 20(a)), are  
 398 quite similar to the ones of the case with vertical component (Figure 20(b)). However, in  
 399 the case with vertical component the relative and residual displacements are systematically  
 400 greater than the case without. By inspecting such time-histories it appears that after the 3rd  
 401 second of simulation (which corresponds more or less to the peak of the seismic input, see

402 Figure 19) the vault's abutments tend to significantly distance themselves until the second 5  
403 of the simulation (which corresponds more or less to a significant decrease of the magnitude  
404 of the seismic input, see Figure 19), and then they tend to stabilize in residual displacements  
405 of several centimeters. Therefore, residual relative displacements have been recorded during  
406 the simulations. Table 4 collects such residual displacements of the vault's abutments at the  
407 end of the dynamic simulation for both the cases with and without the vertical component  
408 of the earthquake. As can be noticed, for both the cases all the sides and diagonals present  
409 an increase of length of more than 3 centimeters, exception made for the side AB which  
410 presents lower elongations.

411 Comparing the computed residual relative displacements of Table 4 with the actual  
412 one obtained by correlating two different surveys conducted before and after the Emilia  
413 earthquake (Table 1), it emerges a quite good agreement between the results even though  
414 the computed relative displacements are quite lower than the actual ones. However, it has  
415 to be pointed out that the vault has been hit by two main seismic shocks, of which the  
416 intensity and the accelerogram of the first one are not available in proximity of the fortress,  
417 and no documentation about the crack pattern of the vault between the May 20th and May  
418 29th 2012 is available. Moreover, by also considering the uncertainties in the measures which  
419 characterize the 1985's survey, with an order of magnitude of some centimeters, the dynamic  
420 simulations results seems reasonably reliable.

421 The damage contour plots provided by the nonlinear dynamic analyses for subsequent  
422 time instants using N-S and E-W components and N-S, E-W and vertical components are  
423 depicted in Figures 21 and 22, respectively. In particular, the simulation time instants at 3s,  
424 4s, 5s and 11s are reported since between 3s and 5s the most significant relative displacements  
425 occur and the instant 11s represents the end of the simulation.

426 As far as it is concerned the damage evolution of the case without vertical component  
427 (Figure 21), after 3s (Figure 21(a)), cracks in the intrados of the vault begin to develop  
428 from the sides parallel to the E-W direction. Then, these cracks evolve and, at 4s (Figure  
429 21(b)), the two limbs tend to link together in the central part. In addition, such limbs  
430 join the extremities of the chimney and, at 5s, they are completely connected creating a  
431 sort of "rectangle" just in front of the chimney (Figure 21(c)). This finding is in good  
432 agreement with the actual crack pattern experienced by the vault, i.e. with the collapse of  
433 the portion (a) which presents a pseudo-rectangular shape, see Figure 5(a). Such cracks are  
434 also present on the extrados, in a very similar way. Moreover, there is very a good agreement  
435 between the crack quasi-perpendicular to the E-W direction, which divides the vault in two  
436 parts, with the actual main crack (b) (Figure 4). Finally, the damage pattern at the end  
437 of the simulation (11s, see Figure 21(d)) is similar to the one at 5s (Figure 21(c)), as also  
438 confirmed by the time-history of the abutments relative displacements of Figure 20 where  
439 no substantial changes of displacements are recorded from 5s to 11s.

440 The damage pattern evolution in the simulation with vertical component (Figure 22)  
441 is similar to the one without vertical component (Figure 21). Indeed, also in this case a  
442 crack in the intrados of the vault arises (Figure 22(a)), which evolves in a sort of rectangle  
443 close to the chimney passing also through the vault in a direction quasi-perpendicular to the  
444 East direction. Therefore, also in this case there is a good agreement with the actual crack

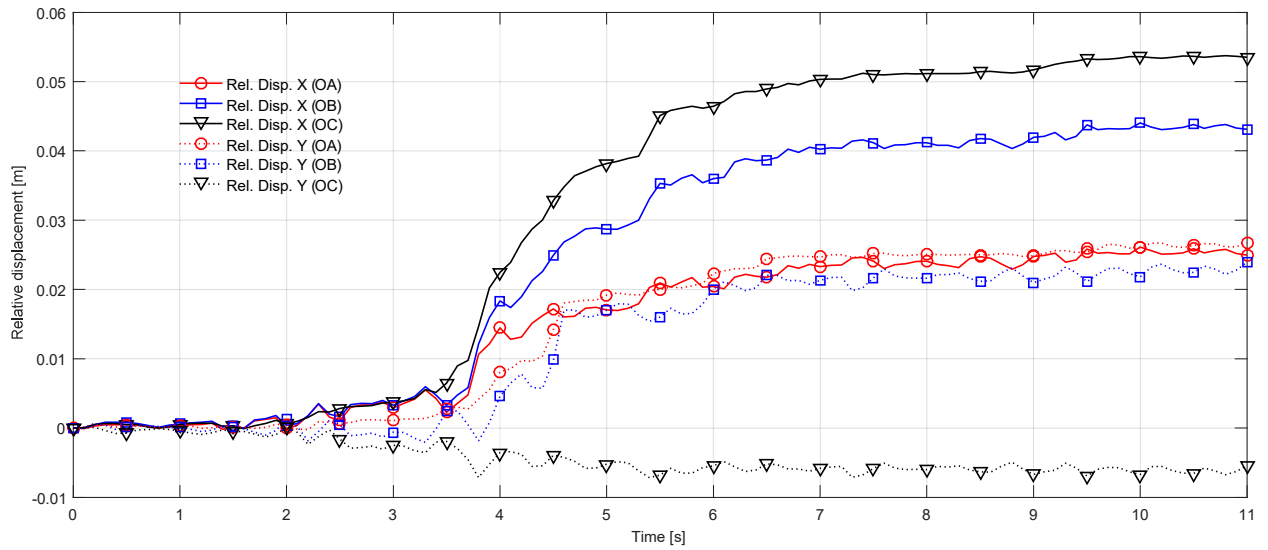
445 pattern. By comparing the damage patterns of the simulations without and with vertical  
 446 component (Figures 21 and 22, respectively) it appears that the latter is slightly wider than  
 447 the first.

448 Finally, it has to be pointed out that, although the failure (a) of Figure 4 seems to be also  
 449 due to a preexisting stairwell, both the dynamic simulations showed a damage pattern which  
 450 tends to cut out a pseudo-rectangular portion of the vault in proximity to the chimney hole.  
 451 Plausibly, this finding could be addressed to the interaction with the chimney hole itself  
 452 (Figure 9(b)), which represents a weakness of the bearing system. Therefore, in the authors  
 453 opinion, the likely presence of a preexisting stairwell (and hence of reshuffled material) in  
 454 such a portion of the vault could have made worse a condition which would already be  
 455 critical, as arisen from nonlinear dynamic analyses.

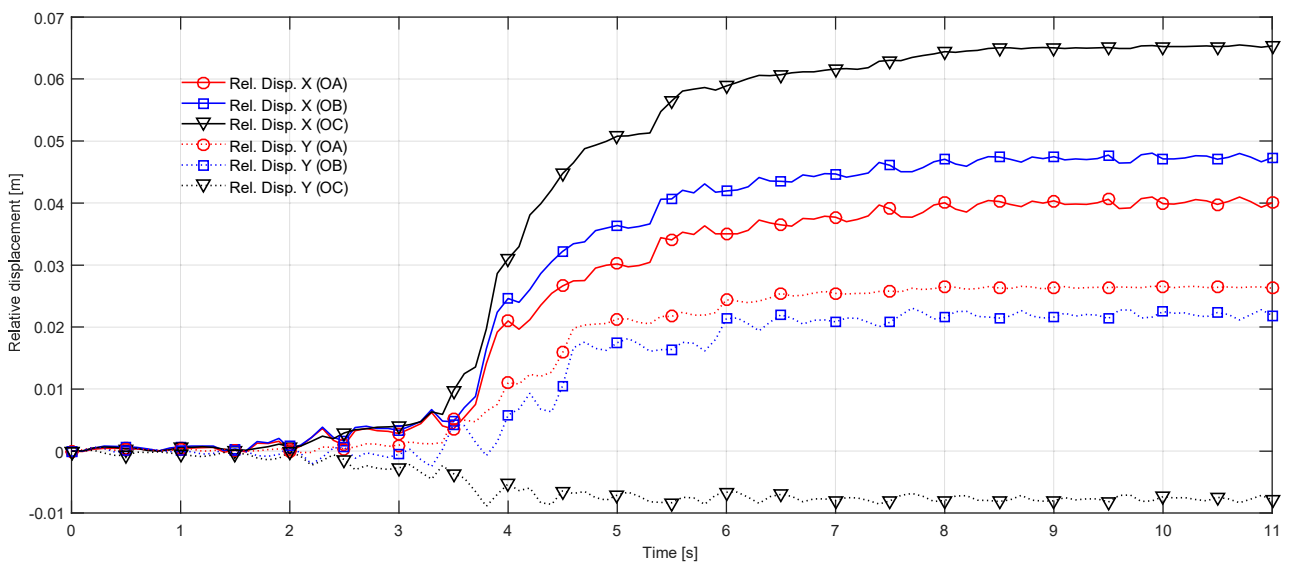
456 Summing up the results, it emerges that the effect of the vertical component of the  
 457 earthquake is not so significant in studying the seismic response of the vault, even if for strong  
 458 vertical components (as the studied case), differently for what occurs for overhang structures  
 459 such as corbels [33]. However, it appears that by considering the vertical component of the  
 460 earthquake in nonlinear dynamic analyses the obtained results are a bit more conservative.

Table 4: Numerical relative displacements of the vault’s abutments at the end of the dynamic simulations.

Without vert. comp.		With vert. comp.	
Rel. displ.	Value	Rel. displ.	Value
$\Delta OA$	3.8 cm	$\Delta OA$	4.9 cm
$\Delta AB$	1.8 cm	$\Delta AB$	0.9 cm
$\Delta BC$	3.1 cm	$\Delta BC$	3.5 cm
$\Delta CO$	5.4 cm	$\Delta CO$	6.6 cm
$\Delta OB$	5.1 cm	$\Delta OB$	5.3 cm
$\Delta CA$	4.3 cm	$\Delta CA$	4.3 cm



(a)



(b)

Figure 20: Vault's abutments relative displacements time-histories measured in nonlinear dynamic analyses: (a) without and (b) with vertical component of the earthquake.

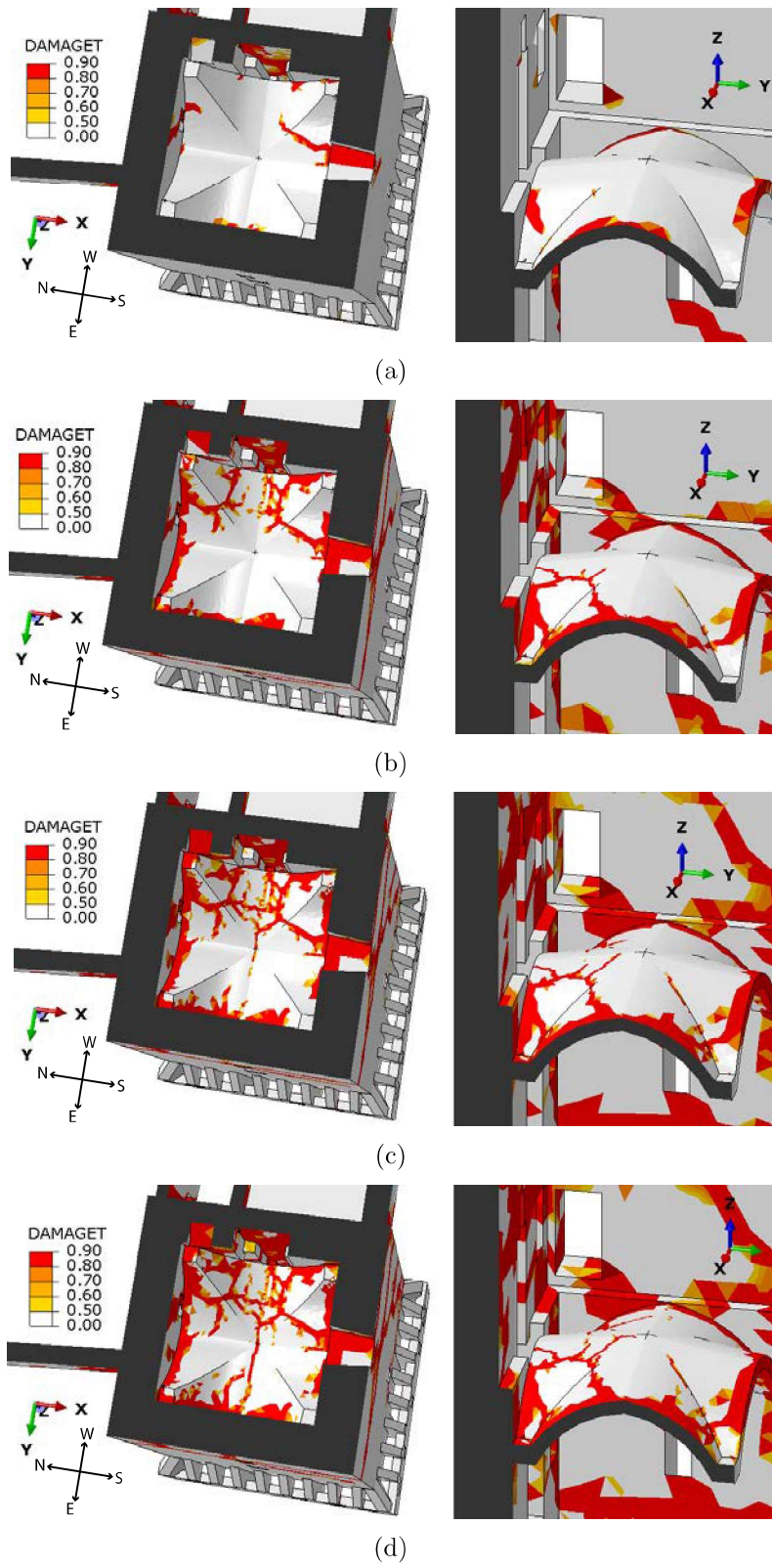


Figure 21: Nonlinear dynamic damage contour plots of the Giulio II Hall's vault, simulation without vertical component. Bottom views (left) and section views (right) at instants (a) 3s, (b) 4s, (c) 5s and (d) 11s.



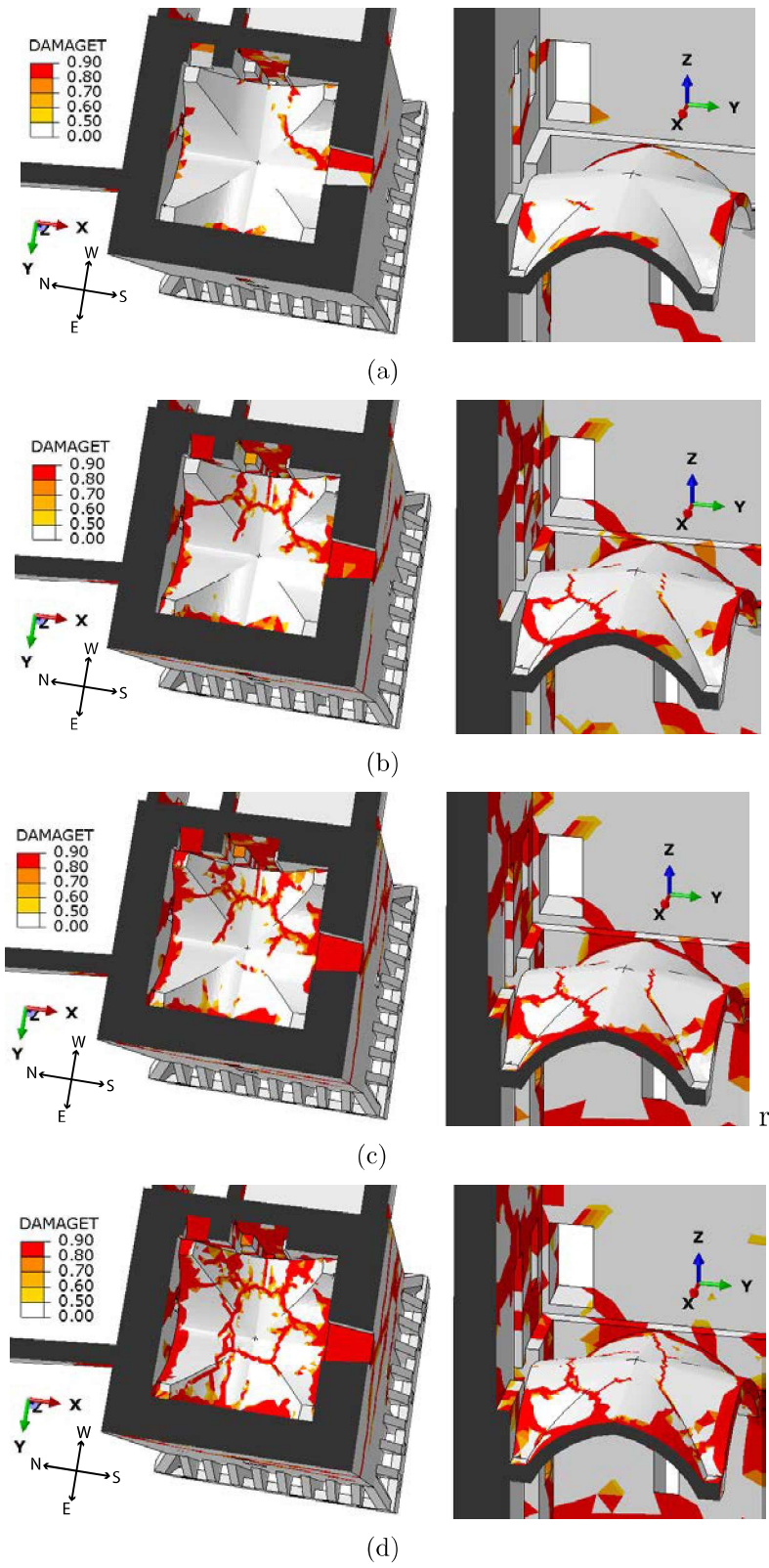


Figure 22: Nonlinear dynamic damage contour plots of the Giulio II Hall's vault, simulation with vertical component. Bottom views (left) and section views (right) at instants (a) 3s, (b) 4s, (c) 5s and (d) 11s.

## 5. Concluding remarks

In this paper, an investigation of the capabilities and limitations of current computational tools to analyze the seismic-induced damage in a masonry vaulted structure has been presented. The case under study was the Giulio II vault, located within the main tower of the San Felice sul Panaro fortress (Italy) which has been severely damaged by the 2012 Emilia earthquake. Attention has been focused on the interaction between the vault and its bearing tower. The developed finite element model included the 3D geometry of the vault within the geometry of the tower, based on a before-quake survey.

Nonlinear static and dynamic analyses have been carried out by using a damage-plasticity constitutive law for masonry. The results have been compared to the vault actual crack pattern as well as to its actual-deformed geometry based on a post-quake laser scanner survey. On the one hand, concerning the damage contour plots, it emerged that both those of nonlinear static and dynamic analyses were in good agreement with the main failures experienced by the vault. Conversely, coarse findings has been obtained with respect to smaller cracks, for which the masonry arrangement, not contemplated in the implemented damage model, plays a more considerable role than for main failures. On the other hand, lower accuracy has been obtained in the prediction of the relative displacements of the vault's abutments. Although nonlinear static analyses are a conventional procedure for the safety evaluation of structures, they are qualitatively able to investigate the main weaknesses of the vault, helping the interpretation of (more comprehensive) dynamic analyses results. Therefore, both nonlinear static and dynamic FE analyses appear to be useful tools for the seismic-induced damage investigation of masonry vaults, and for assessing the main weaknesses of such structures.

Finally, it emerged that the seismic behavior of the tower (and also the presence of adjacent buildings) strongly influence the damage of the vault. Thereby, in order to investigate the seismic-induced damage of a masonry vault, the numerical modeling of the vault should be considered within the model of the bearing structure (walls, columns, etc.), given their mutual remarkable interaction.

## Acknowledgments

The authors would like to thank ABACUS (<http://www.arcoabacus.it>), the municipality of San Felice sul Panaro (MO) and Eng. Stefano Magagnini. Financial support by the Italian Ministry of Education, Universities and Research MIUR is gratefully acknowledged (PRIN2015 "Advanced mechanical modeling of new materials and structures for the solution of 2020 Horizon challenges" prot. 2015JW9NJT\_018).

## References

- [1] Preciado, A. Seismic vulnerability and failure modes simulation of ancient masonry towers by validated virtual finite element models. *Engineering Failure Analysis* 2015, 57, 72-87.
- [2] Clementi, F.; Gazzani, V.; Poiani, M.; Lenci, S. Assessment of seismic behaviour of heritage masonry buildings using numerical modelling. *Journal of Building Engineering* 2016, 8, 2947. doi:10.1016/j.jobe.2016.09.005

- 501 [3] Cattari, S.; Resemini, S.; Lagomarsino, S.. Modelling of vaults as equivalent diaphragms in 3D seismic  
502 analysis of masonry buildings. In Proceedings of 6th international conference on structural analysis of  
503 historic construction, 2008, Bath, UK.
- 504 [4] Çaktı, E.; Saygılı, O.; Dar, E.; Ercan T. Seismic behavior of the Edirnerkapi Mihrimah Sultan Mosque  
505 in Istanbul. In Proceedings of the 6th ECCOMAS Thematic Conference on Computational Methods  
506 in Structural Dynamics and Earthquake Engineering, (Rhodes Island, Greece), 2017.
- 507 [5] Croci G. The Basilica of St. Francis of Assisi after the September 1997 Earthquake. Structural Engi-  
508 neering International 1998, 8(1), 56-58. doi:10.2749/101686698780489667
- 509 [6] S. Huerta. The analysis of masonry architecture: A historical approach. Architectural Science Review  
510 2008, 51(4), 297328.
- 511 [7] M. Como. Statics of historic masonry constructions. Springer-Verlag, Berlin, Germany, 2013.
- 512 [8] Heyman, J. Equilibrium of shell structures, Clarendon Press, Oxford, 1977.
- 513 [9] Heyman, J. The stone skeleton: Structural engineering of masonry architecture. Cambridge University  
514 Press, 1995.
- 515 [10] Chiarugi, A.; Fanelli, A.; Giuseppetti, G. Diagnosis and strengthening of the Brunelleschi Dome. In  
516 Proceedings of IABSE Symposium, 1993, IABSE, Zurich, Switzerland, 441-448.
- 517 [11] Tralli, A.; Alessandri, C.; Milani, G. Computational Methods for Masonry Vaults: A Review of Recent  
518 Results. The Open Civil Engineering Journal 2014, 8(1), 272-287.
- 519 [12] Block, P.; Lachauer, L. Three-Dimensional (3D) Equilibrium Analysis of Gothic Masonry Vaults.  
520 International Journal of Architectural Heritage 2013, 8(3), 312-335. doi:10.1080/15583058.2013.826301
- 521 [13] Andreu, A.; Gil, L.; Roca, P. Computational Analysis of Masonry Structures with a Funicular Model.  
522 Journal of Engineering Mechanics 2007, 133(4), 473-480. doi:10.1061/(asce)0733-9399(2007)133:4(473)
- 523 [14] Fraternali, F.; Angelillo, M.; Fortunato, A. A lumped stress method for plane elastic problems and  
524 the discrete-continuum approximation. International Journal of Solids and Structures 2002, 39(25),  
525 6211-6240. doi:10.1016/s0020-7683(02)00472-9
- 526 [15] D'Ayala, D. F.; Tomasoni, E. Three-Dimensional Analysis of Masonry Vaults Using Limit State  
527 Analysis with Finite Friction. International Journal of Architectural Heritage 2011, 5(2), 140-171.  
528 doi:10.1080/15583050903367595
- 529 [16] Marmo, F.; Rosati, L. Reformulation and extension of the thrust network analysis. Computers &  
530 Structures 2017, 182, 104-118. doi:10.1016/j.compstruc.2016.11.016
- 531 [17] Carini, A.; Genna, F. Stability and strength of old masonry vaults under compressive longi-  
532 tudinal loads: Engineering analyses of a case study. Engineering Structures 2012, 40, 218-229.  
533 doi:10.1016/j.engstruct.2012.02.028
- 534 [18] Theodossopoulos, D.; Sinha, B. P.; Usmani, A. S.; Macdonald, A. J. Assessment of the Structural  
535 Response of Masonry Cross Vaults. Strain 2002, 38(3), 119127. doi:10.1046/j.0039-2103.2002.00021.x
- 536 [19] Creazza, G.; Matteazzi, R.; Saetta, A.; Vitaliani, R. Analyses of Masonry Vaults: A Macro Approach  
537 based on Three-Dimensional Damage Model. Journal of Structural Engineering 2002, 128(5), 646-654.  
538 doi:10.1061/(asce)0733-9445(2002)128:5(646)
- 539 [20] Milani, E.; Milani, G.; Tralli, A. Limit analysis of masonry vaults by means of curved shell finite  
540 elements and homogenization. International Journal of Solids and Structures 2008, 45(20), 5258-5288.  
541 doi:10.1016/j.ijsolstr.2008.05.019
- 542 [21] Milani G.; Valente M.; Alessandri C. The narthex of the Church of the Nativity in Bethlehem: a  
543 non-linear finite element approach to predict the structural damage. Computers & Structures 2017.  
544 In press. Doi: 10.1016/j.compstruc.2017.03.010
- 545 [22] Milani G.; Valente M.; Alessandri C. Advanced numerical insight into the structural damage of ma-  
546 sonry vaults under seismic excitation: two valuable case-studies. International Journal of Masonry  
547 Research and Innovation. In press (forthcoming Vol 2 Issue 2 pages:xx-yy)
- 548 [23] P.B. Lourenço, Computational strategies for masonry structures, Ph.D. Thesis, Delft University Press,  
549 Delft (The Netherlands), 1996.
- 550 [24] Girardi, M.; Padovani, C.; Pellegrini, D. The NOSA-ITACA code for the safety assessment of an-  
551 cient constructions: A case study in Livorno. Advances in Engineering Software 2015, 89, 64-76.

- doi:10.1016/j.advengsoft.2015.04.002
- 552
- 553 [25] Calì, I.; Cannizzaro, F.; Marletta, M. A Discrete Element for Modeling Masonry Vaults. *Advanced*  
554 *Materials Research* 2010, 133-134, 447-452. doi:10.4028/www.scientific.net/amr.133-134.447
- 555 [26] Milani, G.; Rossi, M.; Calderini, C.; Lagomarsino, S. Tilting plane tests on a small-scale masonry cross  
556 vault: Experimental results and numerical simulations through a heterogeneous approach. *Engineering*  
557 *Structures* 2016, 123, 300-312. doi:10.1016/j.engstruct.2016.05.017
- 558 [27] Sarhosis, V.; Bagi, K.; Lemos, J.; Milani, G. *Computational Modeling of Masonry Structures Using*  
559 *the Discrete Element Method*. Hershey, PA: IGI Global, 2016. doi:10.4018/978-1-5225-0231-9
- 560 [28] Castellazzi, G.; D'Altri, A.M.; Bitelli, G.; Selvaggi, I.; Lambertini, A. From Laser Scanning to Finite  
561 Element Analysis of Complex Buildings by Using a Semi-Automatic Procedure. *Sensors* 2015, 15(8),  
562 18360-18380. doi:10.3390/s150818360
- 563 [29] Castellazzi, G.; D'Altri, A. M.; de Miranda, S.; Ubertini, F. An innovative numerical modeling strategy  
564 for the structural analysis of historical monumental buildings. *Engineering Structures* 2017, 132, 229-  
565 248. doi:10.1016/j.engstruct.2016.11.032
- 566 [30] Castellazzi, G.; D'Altri, A.M.; de Miranda, S.; Ubertini, F.; Bitelli, G.; Lambertini, A.; Selvaggi, I.;  
567 Tralli, A. A mesh generation method for historical monumental buildings: an innovative approach.  
568 *ECCOMAS Congress 2016 - Proceedings of the 7th European Congress on Computational Methods*  
569 *in Applied Sciences and Engineering*, 2016, 1, 409-416.
- 570 [31] Degli Abbatì, S.; D'Altri, A.M.; Ottonelli, D.; Castellazzi, G.; Cattari, S.; de Miranda, S.; Lago-  
571 marsino, S. Seismic assessment of complex assets through nonlinear static analyses: the fortress in San  
572 Felice sul Panaro hit by the 2012 earthquake in Italy. In *Proceedings of the 6th ECCOMAS Thematic*  
573 *Conference on Computational Methods in Structural Dynamics and Earthquake Engineering*, (Rhodes  
574 Island, Greece), 2017.
- 575 [32] Forghieri, M.; Bassoli, E.; Vincenzi, L. Dynamic behaviour of the San Felice sul Panaro fortress: Ex-  
576 perimental tests and model updating. In *Proceedings of the 6th ECCOMAS Thematic Conference*  
577 *on Computational Methods in Structural Dynamics and Earthquake Engineering*, (Rhodes Island,  
578 Greece), 2017.
- 579 [33] Castellazzi, G.; D'Altri, A.M.; de Miranda, S.; Magagnini, S.; Tralli, A. On the seismic behavior of  
580 the main tower of San Felice sul Panaro (Italy) fortress. *AIP Conference Proceedings* 2016, 1790(1),  
581 130009. doi: 10.1063/1.4968727
- 582 [34] Castellazzi, G.; D'Altri, A.M.; de Miranda, S.; Chiozzi, A.; Tralli, A. Numerical insights on the seismic  
583 behavior of a non-isolated historical masonry tower. (Submitted).
- 584 [35] Lagomarsino, S.; Cattari, S. PERPETUATE guidelines for seismic performance-based assessment of  
585 cultural heritage masonry structures. *Bulletin of Earthquake Engineering* 2015, 13(1), 13-47.
- 586 [36] Parisi, F.; Augenti, N. Earthquake damages to cultural heritage constructions and simplified assess-  
587 ment of artworks. *Engineering Failure Analysis* 2013, 34, 735-760. doi:10.1016/j.engfailanal.2013.01.005
- 588 [37] Milani, G. Lesson learned after the Emilia-Romagna, Italy, 2029 May 2012 earthquakes: A  
589 limit analysis insight on three masonry churches. *Engineering Failure Analysis* 2013, 34, 761-778.  
590 doi:10.1016/j.engfailanal.2013.01.001
- 591 [38] Milani, G.; Valente, M. Comparative pushover and limit analyses on seven masonry churches dam-  
592 aged by the 2012 Emilia-Romagna (Italy) seismic events: Possibilities of non-linear finite elements  
593 compared with pre-assigned failure mechanisms. *Engineering Failure Analysis* 2015, 47, 129-161.  
594 doi:10.1016/j.engfailanal.2014.09.016
- 595 [39] Milani, G.; Valente, M. Failure analysis of seven masonry churches severely damaged during the 2012  
596 Emilia-Romagna (Italy) earthquake: Non-linear dynamic analyses vs conventional static approaches.  
597 *Engineering Failure Analysis* 2015, 54, 13-56. doi:10.1016/j.engfailanal.2015.03.016
- 598 [40] Dolce, M.; Nicoletti, N.; Ammirati, A.; Bianconi, R.; Filippi, L.; Gorini, A.; Marcucci, S.; Palma,  
599 F.; Zambonelli, E.; Lavecchia, G.; de Nardis, R.; Brozzetti, F.; Boncio, P.; Cirillo, D.; Romano, A.;  
600 Costa, G.; Gallo, A.; Tiberi, L.; Zoppè, G.; Suhadolc, P.; Ponziani, F.; Formica, A. The Emilia thrust  
601 earthquake of 20 May 2012 (Northern Italy): strong motion and geological observations—report I, 2012.  
602 [www.protezionecivile.gov.it/resources/cms/documents/Report\\_DPC\\_1\\_EmiliasEQSd.pdf](http://www.protezionecivile.gov.it/resources/cms/documents/Report_DPC_1_EmiliasEQSd.pdf)

- 603 [41] Dolce, M.; Nicoletti, N.; Ammirati, A.; Bianconi, R.; Filippi, L.; Gorini, A.; Marcucci, S.; Palma, F.;  
604 Zambonelli, E.; Lavecchia, G.; de Nardis, R.; Brozzetti, F.; Boncio, P.; Cirillo, D.; Romano, A.; Costa,  
605 G.; Gallo, A.; Tiberi, L.; Zoppè, G.; Suhadolc, P.; Ponziani, F.; Formica, A. The Ferrara arc thrust  
606 earthquakes of May-June 2012 (Northern Italy): strong-motion and geological observations—report II,  
607 2012. [www.protezionecivile.gov.it/resources/cms/documents/report\\_DPC\\_2\\_EmiliasEQSBis.pdf](http://www.protezionecivile.gov.it/resources/cms/documents/report_DPC_2_EmiliasEQSBis.pdf)  
608 pdf
- 609 [42] Luzi, L.; Hailemikael, S.; Bindi, D.; Pacor, F.; Mele, F. ITACA (ITalian ACcelerometric Archive): A  
610 web portal for the dissemination of Italian strong motion data, *Seismological Research Letters* 2008,  
611 79, 716-722.
- 612 [43] Cattari, S.; Degli Abati, S.; Ferretti, D.; Lagomarsino, S.; Ottonelli, D.; Tralli, A. Damage assessment  
613 of fortresses after the 2012 Emilia earthquake (Italy). *Bulletin of Earthquake Engineering* 2014, 12,  
614 2333-2365.
- 615 [44] Alexander, K. D.; Mark, R.; Abel, J. F. The Structural Behavior of Medieval Ribbed Vaulting. *Journal*  
616 *of the Society of Architectural Historians* 1977, 36(4), 241-251.
- 617 [45] Lengyel, G.; Bagi, K. Numerical analysis of the mechanical role of the ribs in groin vaults. *Computers*  
618 *& Structures* 2015, 158, 42-60.
- 619 [46] Page, A.W. The biaxial compressive strength of brick masonry. In *Proceeding of the Institution of*  
620 *Civil Engineers* 1981, Part 2, 71, 893-906.
- 621 [47] Luciano, R.; Sacco, E. Homogenization technique and damage model for old masonry material. *Inter-*  
622 *national Journal of Solids and Structures* 1997, 34(24), 3191-3208.
- 623 [48] Abaqus®. Theory manual, version 6.14; 2014.
- 624 [49] Lubliner, J.; Oliver, J.; Oller, S.; Oñate, E. A plastic-damage model for concrete. *International Journal*  
625 *of Solids and Structures* 1989, 25(3), 299-326. doi:10.1016/0020-7683(89)90050-4
- 626 [50] Lee, J.; Fenves, G. L. Plastic-Damage Model for Cyclic Loading of Concrete Structures. *Journal of*  
627 *Engineering Mechanics* 1998, 124(8), 892-900. doi:10.1061/(asce)0733-9399(1998)124:8(892)
- 628 [51] Van Der Pluijm. Shear Behaviour of bed joints. In: Abrams DP, editor. *Proceedings of 6th North*  
629 *American masonry conference, Philadelphia, USA, 6-9 June, 1993, 125-136.*
- 630 [52] Valente, M.; Milani, G. Seismic assessment of historical masonry towers by means of simplified ap-  
631 proaches and standard FEM. *Construction and Building Materials* 2016, 108, 74-104.
- 632 [53] Acito, M.; Chesi, C.; Milani, G.; Torri, S. Collapse analysis of the Clock and Fortified towers of Finale  
633 Emilia, Italy, after the 2012 Emilia Romagna seismic sequence: Lesson learned and reconstruction  
634 hypotheses. *Construction and Building Materials* 2016, 115, 193-213.
- 635 [54] DM 14/01/2008. Nuove norme tecniche per le costruzioni. Ministero delle Infrastrutture (GU n.29  
636 04/02/2008), Rome, Italy [New technical norms on constructions].
- 637 [55] Circolare n 617 del 2 Febbraio 2009. Istruzioni per l'applicazione delle nuove norme tecniche per le  
638 costruzioni di cui al decreto ministeriale 14 Gennaio 2008 [Instructions for the application of the new  
639 technical norms on constructions].
- 640 [56] DPCM 9/2/2011. Linee guida per la valutazione e la riduzione del rischio sismico del patrimonio  
641 culturale con riferimento alle Norme tecniche delle costruzioni di cui al decreto del Ministero delle  
642 Infrastrutture e dei trasporti del 14 gennaio 2008 [Italian guidelines for the evaluation and reduction  
643 of the seismic risk of cultural heritage, with reference to the Italian norm of constructions].
- 644 [57] Borri, A.; Cangi, G.; De Maria, A. Caratterizzazione meccanica delle murature (anche alla luce del  
645 recente sisma in Emilia) e interpretazione delle prove sperimentali a taglio. In *Proceedings of ANIDIS*  
646 *Congress, Associazione Nazionale Italiana Di Ingegneria Sismica, 2013, Padua, Italy [Mechanical char-*  
647 *acterization of masonry (considering also the recent Emilia earthquake) and interpretation of shear*  
648 *experimental tests].*
- 649 [58] Pineda, P. Collapse and upgrading mechanisms associated to the structural materials of a deteriorated  
650 masonry tower. *Nonlinear assessment under different damage and loading levels. Engineering Failure*  
651 *Analysis* 2016, 63, 72-93.
- 652 [59] Chiozzi, A.; Simoni, M.; Tralli, A. Base isolation of heavy non-structural monolithic objects at the  
653 top of a masonry monumental construction. *Materials and Structures* 2015, 49(6), 2113-2130.